Pan-Arctic surface ozone: modelling vs measurements

Xin Yang[1], Anne-M. Blechschmidt[2], Kristof Bognar[3], Audra McClure–Begley[4,5], Sara Morris[4,5], Irina Petropavlovskikh[4,5], Andreas Richter[2], Henrik Skov[6], Kimberly Strong[3], David Tarasick[7], Taneil Uttal[5], Mika Vestenius[8], Xiaoyi Zhao[7]

[1]British Antarctic Survey, UK Research Innovation, Cambridge, UK
[2]Institute of Environmental Physics, University of Bremen, Bremen, Germany
[3]Department of Physics, University of Toronto, Toronto, ON, Canada
[4]Cooperative Institute for Research in Environmental Sciences, University of Colorado, Boulder, CO, USA
[5]NOAA Earth System Research Laboratory, Boulder, CO, USA
[6]Climate, Department of Environmental Science, Aarhus University, Denmark
[7]Air Quality Research Division, Environment and Climate Change Canada, Toronto, ON, Canada
[8]Atmopsheric Composition Research, Finnish Meteorological Institute, Helsinki, Finland

Correspondence to: Xin Yang (xinyang55@bas.ac.uk)

Abstract. Within the framework of the International Arctic Systems for Observing the Atmosphere (IASOA), we report a modelling-based study on surface ozone across the Arctic. We use surface ozone from six sites: Summit (Greenland), Pallas (Finland), Barrow (USA), Alert (Canada), Tiksi (Russia), and Villum Research Station (VRS) at Station Nord (North Greenland, Danish Realm), and ozonesonde data from three Canadian sites: Resolute, Eureka, and Alert. Two global chemistry models: a global chemistry transport model (p-TOMCAT) and a global chemistry climate model (UKCA), are used for model-data comparisons. Remotely sensed data of BrO from the GOME-2 satellite instrument and ground-based Multi-axis Differential Optical Absorption Spectroscopy (MAX-DOAS) at Eureka, Canada are used for model validation.

The observed climatology data show that spring surface ozone at coastal sites is heavily depleted, making ozone seasonality at Arctic coastal sites distinctly different from that at inland sites. Model simulations show that surface ozone can be greatly reduced by bromine chemistry. In April, bromine chemistry can cause a net ozone loss (monthly mean) of 10-20 ppbv, with almost half attributable to open-ocean-sourced bromine and the rest to sea-ice-sourced bromine. However, the open-ocean-sourced bromine, via sea spray bromide depletion, cannot by itself produce ozone depletion events (ODEs) (defined as ozone volume mixing ratios VMRs < 10 ppbv). In contrast, sea-ice-sourced bromine, via sea salt aerosol (SSA) production from blowing snow, can produce ODEs even without bromine from sea spray, highlighting the importance of sea ice surface in polar boundary layer chemistry.

Model bromine is sensitive to model configuration, e.g., under the same bromine loading, the total inorganic bromine (Br_Y) in the Arctic spring boundary layer in the p-TOMCAT base run (i.e., with all bromine emissions) can be 2 times larger than that in the UKCA base run. Despite the model differences, both model base runs can successfully reproduce large bromine explosion events (BEEs) in polar spring. Model-integrated tropospheric column BrO generally matches GOME-2 tropospheric columns within ~50% (in the UKCA base run) and factors of 2-3 (in the p-TOMCAT base run). The success of the models in reproducing both ODEs and BEEs in the Arctic indicates that the relevant parameterizations implemented in the models work reasonably well, which supports the proposed mechanism of SSA and bromine production from blowing snow on sea ice. Given that sea ice is a large source of SSA and halogens, changes in sea ice type and extent in a warming climate will influence Arctic boundary layer chemistry, including the oxidation of atmospheric elemental mercury.

1 Introduction

Climatological data show that mean surface ozone across the Arctic is ~5 ppbv higher than that in the Antarctic (Helmig et al., 2007), reflecting the impact of anthropogenic emissions of ozone precursors such as NOx (=NO+NO$_2$) and volatile organic compounds (VOC) in the northern hemisphere (NH) (e.g., Law and Stohl, 2007; Quinn et al., 2008; Walker et al., 2012;

5   Ancellet et al., 2016). For a specific location, the surface ozone depends on multiple factors, including the elevation above sea level (asl), proximity to the coast, human influence, and processes such as photochemical production/loss rates and dry deposition. Over the past several decades, Arctic sea ice extent has been declining (e.g., Cavalier et al., 2012; Laxon et al., 2013, Olonscheck et al., 2019) and thinning (Lindsay and Zhang 2005; Kwok and Rothrock, 2009). The rapid disappearance of summer multiyear sea ice means there will be more young sea ice in the following winter and spring, which will potentially

10   affect the exchange of chemical compounds (both gaseous and particulate phase) between the ocean, sea ice, and the atmosphere. A modelling study shows that the alteration of surface albedo alone, in a scenario of a sea-ice-free Arctic summer, can significantly alter the atmospheric oxidizing capacity at high latitudes, including the concentrations of ozone and the hydroxyl radical (OH) (Voulgarakis et al., 2009).

Polar boundary layer ozone at coastal sites in both hemispheres is affected by spring-time ozone depletion events (ODEs),

15   with ozone VMRs < 10 ppbv (Bottenheim et al., 1986; Barrie et al., 1988). ODEs are mostly found in association with strongly enhanced bromine, so-called bromine explosion events (BEEs). The enhanced bromine monoxide (BrO) can extend from near the surface to a height of a few km, as has been frequently observed by in situ measurements (e.g., Liao et al., 2011, 2012; Buys et al., 2012; Schultz et al., 2017 and references therein), ground-based remote sensing (e.g., MAX-DOAS, Frieβ et al, 2011; Zhao et al., 2016) and satellite-based remote sensors (e.g., Wagner and Platt, 1998; Theys et al., 2011). Analyses of

20   Arctic transport (Bottenheim and Chan 2006; Liu et al., 2013), as well as in situ measurements (Bottenheim et al., 2009; Jacobi et al., 2010; Seabrook et al., 2013) suggest that the near-surface ozone minimum in spring is not limited to coastal sites, but covers much of the Arctic basin, indicating that the sources of bromine are mainly sea-ice-related (e.g., Simpson et al. 2007a, Abbatt et al., 2012). However, the dominant sources of bromine during ODEs or BEEs are still under debate. Proposed candidates for bromine release include e.g., frost flowers (Kaleschke et al. 2004), first-year sea ice (Skov et al., 2004; Simpson

25   et al., 2007b), sea salt aerosol (SSA) produced from blowing snow (Yang et al., 2008), snowpacks (Pratt et al., 2013), and stratospheric BrO intrusions (Salawitch et al., 2010). Global chemical models have been used to test chemical schemes for interpreting or reproducing observed spring ODEs and BEEs. For instance, Toyota et al. (2011) and Falk and Sinnhuber (2018) focused on snowpack-released bromine while Yang et al. (2010) and Choi et al. (2012; 2018) considered blowing-snow-sourced bromine. Box (or 0-D) models are used for process studies such as heterogeneous reactions on various saline particles

30   including SSA, frost flowers, and snowpack (Fan and Jacob 1992; Tang and McConnell, 1996; Michalowski et al. 2000; Evans et al., 2003). 1-D models have also been developed with a focus on the exchange of gaseous-phase halogens between the air in the boundary layer and the snowpack, and boundary layer ODEs and BEEs (Saiz-Lopez et al., 2008; Thomas et al., 2011, 2012; Cao et al. 2013; 2016).

Recent winter cruise data from the Weddell Sea confirm that the sea ice surface is a large source of sea salt aerosol (Frey et

35   al., 2019; Yang et al., 2019). Like the open-ocean-sourced sea spray, the sea-ice-sourced SSA is also a large reservoir of various chemical compounds, including inorganic halogens. Through heterogeneous reactions, bromide (Br$^-$) and chloride (Cl$^-$) can be activated and released to the air to form a large source of inorganic halogens (Fan and Jacob, 1992, Vogt et al., 1996), and the consequences may induce polar boundary layer bromine explosion events and ozone depletion events (Simpson et al., 2007a; Abbatt et al., 2012).

40   SSA bromide data collected in the NH mid-to-low latitudes show that bromide is largely depleted with respect to sodium without a clear seasonal cycle of the depletion strength (Sander et al., 2003). This is attributed to the air pollution and acidification of SSA in the NH. However, in the Southern Ocean of Antarctica, where the air is less polluted, a seasonally varying bromine depletion strength is observed (Ayers et al., 1999, Legrand et al., 2016) with maximum depletion factors in

later spring to early summer and a minimum in winter. Global chemistry models with a detailed tropospheric bromine scheme show that open-ocean-sourced bromine can cause tropospheric ozone loss of ~5% at mid- to-low latitudes and up to 15-30% at high latitudes (Yang et al., 2005; Parrella et al., 2012). Model runs with sea-ice-sourced bromine implemented show that an additional 10-25% ozone loss can be simulated in polar spring (Yang et al., 2010). Global models with a relatively coarse

5 horizontal resolution of a few degrees by a few degrees can explain large-scale (e.g., > ~500 km) ODEs and BEEs in both polar regions (Theys et al., 2011; Zhao et al., 2016; Legrand et al. 2016; Choi et al., 2018). However, no systematic validation against measured ozone and BrO in the Arctic and the Antarctic has been presented. This is important to examine and refine the bromine scheme implemented in models, especially in the polar regions.

Most current global-scale chemistry models do not have sea-ice-sourced halogens included. A recent assessment of

10 tropospheric ozone performance in current global models is mainly focused on mid-latitudes (Young et al., 2018), as are most global ozone seasonality studies (e.g., Derwent et al., 2016; Parrish et al., 2016). Thus, relatively little is known about model skill in reproducing polar boundary layer ozone, leaving a large gap in our understanding of the global ozone budget in the polar regions.

Although observations of surface ozone and tropospheric vertical ozone profiles are limited in the Arctic, existing data clearly

15 show that there is a spring ozone maximum at inland sites such as Pallas (e.g., Hatakka et al., 2003) and Summit, Greenland (3208 m asl) (e.g., Helmig et al., 2007). It has been proposed that this spring ozone maximum, also seen at other high-latitude locations (e.g., Monks et al., 2000), is attributable to reduced ozone photo-dissociation and dry deposition in winter, balanced by increased stratospheric ozone intrusions in spring following the breakup of the polar vortex in the lower stratosphere (e.g., Laurila 1999; Helmig et al., 2007). However, at coastal sites, ozone is observed to be heavily depleted during spring. Moreover,

20 the near-surface ozone minimum observed in spring is not limited to coastal sites, but covers much of the Arctic boundary layer (Liu et al., 2013). Can global models with state-of-the-art bromine chemistry reproduce this pan-Arctic spring ozone depletion? What is the dominant factor that causes spring ODEs and BEEs? These are the two key questions addressed in this study.

We employ multi-year integrations in two global chemistry models (the p-TOMCAT chemistry transport model and the UKCA

25 chemistry-climate model) and perform comparisons to observations of surface ozone, vertical ozone profiles, and GOME-2 tropospheric column BrO, in order to validate model parameterizations, including both SSA production and bromine release. This work is undertaken in the framework of International Arctic Systems for Observing the Atmosphere (IASOA), whose mission is to advance coordinated and collaborative research objectives using data from independent Arctic atmospheric observatories (Uttal et al. 2016). This is a modelling-based study of the pan-Arctic surface zone; more information about ozone

30 climatology can be found in a companion paper by McClure–Begley et al. (in preparation). The surface ozone climatology data used in this study are from Summit, Greenland (72.6°N, 38.5°W), Pallas, Finland (68.0°N, 24.1°E), Barrow, USA (71.3°N, 156.6°W), Alert, Canada (82.5°N, 62.3°W), Tiksi, Russia (71.6°N, 128.9°E) and Villum Research Station (VRS), at Station Nord, Greenland (81.4°N, 16.4°W). Ozonesonde data are from three Canadian sites: Resolute (74.7°N, 95.0°W), Eureka (80.1°N, 86.4°W), and Alert. Retrievals of tropospheric column BrO from the GOME-2 instrument, including maps and

35 subsetted data for each site, and ground-based MAX-DOAS BrO at Eureka are also used. Figure 1 shows the locations of these sites. Measurements are described briefly in Section 2. Model experiments are described in Section 3. The results and discussions of the model-data comparison are presented in Sections 4 and 5, respectively.

2 Measurements

2.1 Surface ozone and ozonesondes

40 Surface ozone data are retrieved from the World Data Centre for Reactive Gases (WDCRG). The measurements of surface ozone are made by several brands of dual cell UV absorption monitors, which relate UV absorption to ozone concentration

following the Beer-Lambert law. Details can be found in these articles: e.g., VRS Research Station in Skov et al. (2004, 2019), Alert in Bottenheim et al. (2002), or in review articles by e.g., Gaudel et al. (2018), Oltmans et al. (20100) and Cooper et al. (submitted). In general, the technique has a detection limit of about 1 ppbv and an uncertainty (95% confidence interval) of about 1 ppbv for VMRs below 10 ppbv and about 2 ppbv for more typical surface VMRs of 30-40 ppbv (Galbally et al., 2013;

5 Tarasick et al., 2019a).

Ozonesonde data from the three Canadian stations used here can be found at the World Ozone and Ultraviolet Radiation Data Centre (WOUDC). During the period of interest here all ozonesondes used electrochemical concentration cells (ECC) (Komhyr, 1969), manufactured by Environmental Science (EN-SCI) Corp. All used the conventional neutral-buffered 1% potassium iodide sensing solution. The data records of the Canadian sites have recently been re-evaluated (Tarasick et al.,

10 2016). Based on the typical ozone sensor response time of 25-40 s (Smit and Kley, 1998), and assuming a typical balloon ascent rate of 4-5 m s^{-1}, the ozonesondes have a vertical resolution of about 100-200 metres. Measurement precision is ±3-5% and the overall uncertainty in ozone VMRs is less than 10% in the troposphere (Kerr et al., 1994; Smit et al., 2007; Tarasick et al., 2016; 2019a, c).

Ozonesonde releases are normally once per week, although additional releases are often scheduled during observational

15 campaigns in the Arctic spring. Despite their low frequency of observation compared to surface monitoring, ozonesondes have been used successfully to study boundary-layer processes like ODEs (e.g., Bottenheim et al., 2002; Tarasick and Bottenheim, 2002) and long-range transport (e.g., Oltmans et al., 2010; He et al., 2011; Tarasick et al., 2019b).

2.2 Complementary data sets

In addition to the ozone measurements, several other data sets are employed in this study: tropospheric columns of BrO from

20 the Global Ozone Monitoring Experiment-2 (GOME-2; Callies et al., 2000) instrument onboard the Meteorological Operational Satellite-A (MetOp-A), and lower tropospheric profiles of BrO from ground-based Multi-axis Differential Optical Absorption Spectroscopy (MAX-DOAS) at Eureka, Canada.

The GOME-2 tropospheric BrO columns used in this study are described in further detail by Blechschmidt et al. (2016). In summary, tropospheric BrO vertical columns (VCD$_{trop}$) were obtained based on the approach of Begoin et al. (2010) for

25 deriving BrO total slant column densities by the DOAS (Platt et al., 1994) method using a 336-347 nm fitting window (Afe et al., 2004) and on Theys et al. (2011) for stratospheric correction. The latter involves the use of a climatology of stratospheric vertical column densities (VCDs) of BrO estimated by the BASCOE chemical transport model (Errera et al., 2008; Viscardy et al., 2010). The stratospheric VCDs were converted to slant columns by application of a stratospheric air mass factor and then subtracted from total slant columns. A tropospheric air mass factor was applied for conversion to VCD$_{trop}$ assuming that

30 all BrO is located and well mixed within the lowermost 400 m of the troposphere over ice or snow with a surface spectral reflectance of 0.9. A sensitivity study for a BEE case showed that the GOME-2 tropospheric BrO column has a moderate sensitivity to the stratospheric BrO column, e.g., a variation in the VCD$_{strat}$ of 15–30% leads to a change in VCD$_{trop}$ of about 0.5 to 1×10^{13} molecules cm^2, respectively (Zhao et al., 2016). The influence of clouds on GOME-2 BrO retrievals and the implications for studying bromine explosion events using GOME-2 data are discussed in Blechschmidt et al. (2016). GOME-

35 2 tropospheric BrO column maps (0.5x0.5 degree grid) and time series based on subsetted data of VCD$_{trop}$ (all measurements having their centre within a distance of <40 km from the ground-station) at Resolute, Eureka and Alert sites are used here. MAX-DOAS measurements were performed at the Polar Environment Atmospheric Research Laboratory (PEARL) Ridge Laboratory (610 m) in Eureka. Spectra were recorded in the UV using a grating spectrometer (1200 groves/mm grating) with a cooled (200 K) charge-coupled device (CCD) detector at 0.4-0.5 nm resolution. Elevation angles of 30°, 15°, 10°, 8°, and 5°

40 (6° in 2011) were used in the elevation scans, and measurements were only taken with solar elevation above 4°. Differential slant column densities (dSCDs) of BrO and the oxygen dimer (O$_4$) were retrieved using the settings described in Zhao et al. (2016). Reference spectra for the DOAS analysis were interpolated from zenith measurements taken before and after each

elevation scan. dSCDs were converted to profiles using a two-step optimal estimation method (Frieβ et al, 2011). First, aerosol extinction profiles were retrieved from O_4 dSCDs, and then the extinction profiles were used as a forward model parameter in the BrO retrieval. The retrievals were performed on a 0-4 km grid with 0.2 km resolution. Due to the altitude of the instrument (610 m) and the lack of low or negative elevation angles, the retrieved profiles have limited sensitivity to the surface.

3 Models

A global chemistry transport model, p-TOMCAT, and a global chemistry climate model, UKCA, are used in this study. For comparisons with the ozone and BrO measurements, both models are driven by 6-hourly ERA-Interim data (temperature, wind, and humidity) for specific years. The ERA-Interim data were obtained from the European Centre for Medium-Range Weather Forecasts (ECMWF) (Dee et al., 2011). In addition to the two global chemistry models shown below, we used back-trajectories from the NOAA Hybrid Single-Particle Lagrangian Integrated Trajectory (HYSPLIT) model (Stein et al., 2015; Rolph et al. 2017) for air-mass history study of the selected ODE case in section 4.2.

3.1 p-TOMCAT model

The Cambridge parallelised-Tropospheric Offline Model of Chemistry and Transport (p-TOMCAT) is a chemistry transport model (CTM) (O'Connor et al., 2005), with a horizontal resolution of 2.825° × 2.825° (longitude × latitude) and 31 vertical layers from the surface to about 10 hPa at the top layer. Sea-ice coverage and sea surface temperatures are monthly and taken from the Hadley Centre Sea Ice and Sea Surface Temperature dataset (Rayner et al., 2003). The p-TOMCAT model uses the Holtslag and Boville (1993) non-local vertical diffusion scheme from the National Centre for Atmospheric Research Community Climate Model, Version 2. This scheme determines the planetary boundary layer (PBL) height explicitly and takes account of large-scale eddy transport that can occur throughout the boundary layer even when part of it is statically stable. Implementation and validation of the PBL scheme was carried out by Wang et al. (1999). The convective mass flux scheme applied to the model is based on Tiedtke et al. (1989). The model behaviour in terms of vertical mixing of atmospheric tracer and air mass transport has been reported in Russo et al. (2011) and Ruti et al. (2011).

The ozone photochemistry scheme applied to the model has been detailed in previous studies (Law et al., 1998, 2000). Ozone is dry-deposited in the bottom model layer with dry deposition velocity inferred from the study of Ganzeveld and Lelieveld (1995) by Giannakopoulos (1998). The original dry deposition velocity over ocean and snow (=0.05 cm s^{-1}) is reduced to 0.01 cm s^{-1} in this study following recent work by Hardacre et al. (2015) and Luhar et al. (2018).

The tropospheric halogen chemistry scheme implemented follows the initial work by Yang et al. (2005, 2010) plus updates to deposition schemes (wet and dry) reported in Legrand et al. (2016). Tropospheric bromine comes from three emission sources: (i) very short-lived substances (VSLS) bromocarbons following the work of Warwick et al. (2006) with reduced flux for CH_2Br_2 (Yang et al., 2014), (ii) Open ocean sea spray (Yang et al. 2005, Breider et al., 2009; Parrella et al., 2012), and (iii) sea-ice-sourced SSA in polar regions following the work of Yang et al. (2008; 2010; 2019).

A process-based SSA transport, dry and wet deposition scheme has been implemented in the model by Levine et al. (2014) based on the work of Reader and McFarlane (2003). The open ocean sea spray emission scheme follows Jaeglé et al., (2011), and the sea-ice-sourced SSA scheme follows the latest work of Yang et al. (2019). Both open-ocean-sourced and sea-ice-sourced SSA (denoted as OO and SI, respectively) are tagged in 21 size bins covering dry NaCl diameter of 0.02-20 μm in order to track their history for online calculation of their surface density for heterogeneous reaction rates.

Below are some specific parameters applied in this study for the Arctic SSA simulation, which are slightly different from previous runs. For instance, a full distribution of surface snow salinity taken from the Weddell Sea cruise data (Frey et al., 2019) is used, instead of a constant value (=0.3 psu, practical salinity unit) that was used in Legrand et al. (2016) and Zhao et al. (2017). For the Arctic, snow salinity is assumed to be 3.5 times the Weddell Sea salinity, rather than 2 times as used in

Rhodes et al. (2016). A mean snow age of 3 days is used for the Arctic following the recent work of Huang and Jaeglé (2017). We assume that the evaporation rate of blowing snow particles is controlled by the moisture gradient between the surface of the particle and the ambient air, i.e., the classic mechanism in Yang et al. (2019). Other physical parameters include blowing snow size distribution (a shape parameter $\alpha=3$ and a scale parameter $\beta=37.5$ μm), SSA production ratio N =20 (i.e., 20 SSA
5   particles formed from one saline wind-blown snow particle during sublimation).

To parameterize bromine release from SSA in the Arctic, two different patterns of bromine depletion factor (DF) are used. Table 1 contains a seasonal DF scheme with a maximum value of 0.53 in May and a minimum of 0.07 in December. This seasonal scheme is derived from the bulk SSA bromide depletion strength from Dumont d'Urville (Legrand et al., 2016), Cape Grim and Macquarie Island (Ayers et al., 1999) in the Southern Hemisphere with a six-month shift of the phase in order to
10 apply to the NH. Since similar year-round in situ data from the Arctic is not available, we could not justify this seasonal DF pattern, which demands further systematic measurements in the Arctic. As used in previous modelling studies, a non-seasonal (size-dependent) DF scheme for the NH is used for comparison (Supplementary Table 1), which is derived from previous work of Yang et al. (2008, 2010) and Breider et al. (2009). Note that we simply apply these DF schemes to all SSA emitted and do not distinguish between the open-ocean-sourced and the sea-ice-sourced SSA in terms of bromine release. However, this
15 approach may introduce bias as freshly emitted sea spray is alkaline with pH>8 and needs acidification first by absorbing sulphate or nitrate before bromide can be liberated to the atmosphere through heterogeneous reactions (e.g., Breider et al., 2009). In contrast, snowpack in the Arctic is largely acidified with pH of 4-6 due to local acidity contamination (e.g., de Caritat et al., 2005). Thus the difference in initial conditions between sea spray and sea-ice-sourced SSA may affect bromine release in both timing and strength, which has not been considered by our models.

20 **3.2 UKCA**

UKCA, a version of the UK Earth System Model with Chemistry and Aerosols, has a dynamical core from the Met Office Unified Model (UM) (Morgenstern et al., 2009). Model version-7.3 is used in this study with a horizontal resolution of 3.75° × 2.5° and 60 vertical layers from the surface to ~84 km. In this study, a nudged version is used to ensure a model meteorological field close to the real situation for data-model comparison. The tropospheric chemistry scheme was built on
25 the scheme in p-TOMCAT model, but has since developed differently and now contains a comprehensive stratospheric chemistry scheme for climate studies (Braesicke et al., 2013; Banerjee et al., 2014). In terms of SSA production, the same schemes for open ocean sea spray and for sea-ice-sourced SSA as in the p-TOMCAT are used, apart from the fact that the SSA in UKCA runs is no longer being tagged and tracked for online calculation of heterogeneous reaction rates. Therefore, the emitted SSAs are just used for bromine emission. For heterogeneous reactions, the aerosol surface area density is calculated
30 using the monthly climatology aerosol dataset taken from the CLASSIC scheme (Johnson et al., 2010).

Note that UM-UKCA is a complex chemistry-climate coupling model, covering the whole atmosphere including both troposphere and stratosphere. In many aspects of dynamics and chemistry, it behaves quite differently from the p-TOMCAT CTM. A detailed comparison of model characteristics in vertical mixing and transport of tropical boundary layer tracers was performed by Russo et al. (2011) and Hoyle et al. (2011). The bottom model layer of UKCA, in which chemical compounds
35 such as ozone undergo dry deposition, is ~20 m thick, while in p-TOMCAT it is ~60 m thick. All released SSA and bromine (in the form of Br_2) are put in the bottom model layer before they are further vertically mixed and horizontally transported. These differences in model vertical resolution may affect model output even if other factors are the same. Although the two models are quite different, e.g., in absolute values of chemical compounds, the relative changes in response to changes of bromine loading, for example, are still informative and will be our major interest and focus of the discussion.

3.3 Model experiments

Table 2 lists model experiments performed in this study. The two model base runs, pTOMCAT_SI_OO_VSLS and UKCA_SI_OO_VSLS, contain bromine emissions from both sea-ice-sourced and open-ocean-sourced SSA and VSLS bromocarbons. The pTOMCAT_No_Br run does not include any bromine emission, therefore, it is a model run without

5 bromine chemistry. The pTOMCAT_VSLS and UKCA_VSLS runs only contain bromocarbons as a source of bromine (without bromine from open ocean and sea ice). The pTOMCAT_SI_VSLS and UKCA_SI_VSLS runs only contain sea-ice-sourced bromine and bromocarbons as sources of bromine. Similarly, the pTOMCAT_OO_VSLS and UKCA_OO_VSLS runs only contain sea-spray-sourced bromine and bromocarbons. By checking the differences between experiments from the same model, we expect to separate individual bromine source contributions to Arctic boundary layer bromine and ozone change.

10 Similarly, by checking the differences between the two model responses, we will see model-induced uncertainty, e.g., in both the bromine budget and ozone loss. This is because both models employ very similar bromine emissions. Therefore, the differences are mainly due to different model set-ups either in their physical aspect, including precipitation, boundary layer dynamics, land use, etc, or in their chemistry aspect involving key atmospheric species such as ozone or OH. Given that both models used in this study share a very similar tropospheric bromine-chemistry scheme, it is likely that the major factor causing

15 model-to-model differences is in the physical set-up, rather than the chemical set-up. This is reasonable given that p-TOMCAT is a CTM while UKCA is a GCM.

Apart from the pTOMCAT_Fixed_DF run, in which a fixed (non-seasonal) DF scheme is used (Table S1), all model experiments apply the same bromine DF scheme shown in Table 1. A multiple-year integration (2006-2008) is performed, with averaged outputs used as a climatology for comparison. Several spring runs in 2010, 2011 and 2013 are made with more

20 frequent outputs for ODE and BEE comparisons: 1-hourly output frequency in pTOMCAT_SI_OO_VSLS and 3-hourly output frequency in UKCA_SI_OO_VSLS are used for further analysis and model-data comparisons. These years are selected because either significant ODEs or BEEs are observed at one or more sites.

4 Results

4.1 Surface ozone seasonality

25 Figure 2 shows observed monthly mean surface ozone VMRs at the six Arctic locations, two inland (Summit and Pallas) and four coastal (Alert, Barrow, Tiksi and VRS) sites. Spring ozone maxima of >50 ppbv at Summit and ~45 ppbv at Pallas were observed. However, at coastal sites, spring-time ozone is depleted, with minimum VMRs of 15~20 ppbv, which are comparable to or even lower than their summer ozone minimum in July-August. The summer minimum is thought attributable to enhanced ozone photo-dissociation, where NO_X levels are low, and increased dry deposition to plants (e.g., Hatakka et al., 2003). At

30 higher latitude sites such as Alert and VRS, that are within the polar dome and surrounded by Arctic tundra with sparse vegetation, there is normally still snow coverage even in mid-summer, so the local effect of dry deposition to plants may not be as significant as at Pallas or other sites located in the south. However, the long-range transport from lower latitudes of ozone affected by summer plants may result in vegetation having an effect on these sites. Figure 2 also shows that model runs without bromine chemistry (pTOMCAT_No_Br) and with bromocarbons only (pTOMCAT_VSLS) can generate spring ozone maxima

35 at all six sites. When open-ocean-sourced Br is included (orange line in Fig. 2), the spring ozone peak is reduced significantly. The OO-sourced bromine can cause ozone reductions in all seasons (Fig. 3), with a maximum reduction of > 10 ppbv in April and a minimum reduction (1~2 ppbv) in summer. However, the OO-sourced bromine will not alter the ozone seasonality pattern, as the spring ozone peak remains (Fig. 2). On the other hand, sea-ice-sourced bromine (red line in Fig. 2) can significantly perturb the ozone seasonal cycle, by removing the spring ozone peak completely. On average, SI-sourced bromine

40 can cause a maximum ozone loss of > 10 ppbv in April at coastal sites (Fig. 3), similar to the OO-sourced bromine effect. In autumn, SI-sourced bromine only weakly influences the bromine budget and ozone loss. Model runs which contain bromine

sources from both OO and SI (black line in Fig. 3) can cause a maximum ozone loss of > 25 ppbv (in monthly mean) in April at coastal sites, giving the best match to the observations (Fig. 2).

A similar effect of the SI- and OO-sourced bromine on surface ozone can be seen in UKCA runs but with net ozone loss only half of that seen in p-TOMCAT runs (Fig. S1). As discussed below, this difference is consistent with the difference in total

5   inorganic bromine (Br$_Y$=HOBr +HBr +BrO +Br +BrONO$_2$ +BrNO$_2$ +2XBr$_2$ +BrCl) between the two models: a spring surface layer Br$_Y$ maximum of 10-30 pptv is simulated in pTOMCAT_SI_OO_VSLS (Fig. 3), which is about twice that (5-10 pptv) in UKCA_SI_OO_VSLS (Fig. S1). Since both models employ a very similar bromine emission flux (e.g., SSA production driven by ECMWF wind fields and with the same bromine depletion factor), the difference in Br$_Y$ between the two models is likely due to the difference in removal process of inorganic bromine species, such as HBr, HOBr, Br$_2$ and BrONO$_2$, which are either

10   dry and/or wet deposited. Previous model simulations have shown that, on the global scale, precipitation wash-out is responsible for ~90% of the removal of tropospheric Br$_Y$ (Yang et al., 2005). In polar regions, where the precipitation rate is relatively low, dry deposition to the surface is an efficient pathway for inorganic bromine removal. In addition, the different approaches in chemical scheme applied by the models may also affects inorganic bromine deposition rate through influencing partitioning of inorganic bromine species. This is because some species (e.g., HBr, HOBr) are very soluble while others are

15   not (e.g., BrO). A higher BrO partitioning is expected at a higher ozone concentration, and vice versa. Therefore, an overestimated ozone is expected to have a negative feedback to bromine removal and net ozone loss via bromine chemistry. Comparing the BrO/Br$_Y$ ratio between the two models (Fig. S2), we can see that both UKCA_SI_OO_VSLS and pTOMCAT_SI_OO_VSLS give a very similar spring peak with a ratio around 20-30% at coastal sites, with an exception at VRS, where a ratio of up to >60% is simulated in the UKCA_SI_OO_VSLS run. The largest discrepancy appears in summer

20   at some costal sites such as Alert, Tiksi and VRS, where a second summer peak ratio is simulated in the UKCA_SI_OO_VSLS run, which is likely attributed to the obviously overestimated summer ozone concentrations by this model (Fig. S3).

From Fig. 2 and Fig. S1 we can see that, on average, surface BrO VMRs at inland sites are smaller than that at coastal sites in both model outputs. For example, in April, mean BrO is ~1 pptv at Summit and ~0.5 pptv at Pallas, at coastal sites, VMRs are between 2 and 7 pptv in pTOMCAT_SI_OO_VSLS run. In terms of Br$_Y$, as shown in Fig. 3, in April, both OO- and SI-

25   sourced bromine contributes roughly the same amount (6~8 pptv) at the two inland sites of Summit and Pallas. At coastal sites (Alert, Barrow, Tiksi and VRS), the OO-sourced bromine contributes one-sixth to half of the SI-sourced Br$_Y$, i.e., 4~5 pptv vs 8~30 pptv. The large (and small) gradient in Br$_Y$ of the SI-sourced (and the OO-sourced) bromine between inland and coastal sites indicates that SI-sourced bromine is locally sourced, while OO-sourced bromine is remotely transported and thus has a smaller horizontal gradient in VMR. In addition, VSLS bromocarbons only have a relatively small contribution of ~0.5 pptv

30   Br$_Y$ in summer (Fig. 3), but this corresponds to an ozone loss of ~1 ppbv.

4.2 Surface ozone frequency distribution

Figure 4 shows NH summer (July) surface ozone frequency distribution at four coastal sites from both observation and p-TOMCAT runs. Climatology clearly indicates a single ozone peak distribution with peak VMRs around ~20 ppbv. The p-TOMCAT model successfully reproduces this summer single peak distribution frequency, though it overestimates it by a few

35   ppbv, e.g., at Alert and VRS. Similar to what is reflected in Fig. 3, the bromine effect on ozone loss is small, only 1-2 ppbv. In April, the observed ozone distribution frequency is quite different from the summer pattern, as a flat distribution across ozone bins is observed with a large ozone depletion fraction at ozone VMRs <10 ppbv (Fig. 5). Although both p-TOMCAT (Fig. 5) and UKCA (Fig. S4) fail to reproduce this flat distribution pattern, the two model runs with SI-sourced bromine implemented can largely reproduce ozone depletion fraction. It is interesting to note that though OO-sourced bromine alone

40   can cause April monthly mean ozone to drop by 5~10 ppbv at coastal sites (dashed blue line vs solid blue line in Fig.5), but itself alone cannot generate any ozone depletion at VMRs < 20 ppbv, indicating that this remotely sourced bromine to the Arctic is not responsible for coastal ODEs; rather, it only affects background ozone. On the other hand, SI-sourced bromine

can cause ozone depletion with a significant fraction of ozone VMRs < 10 ppbv (dashed orange line in Fig. 5 and Fig. S4), supporting the suggestion that locally sourced bromine (from sea ice) is responsible for spring ODEs.

As discussed in Section 4.3, the failure of models in reproducing the flat ozone distribution in spring is likely attributable to the coarse resolution of the models used. For instance, the ~2.8°×2.8° in p-TOMCAT and 3.75°×2.5° in UKCA horizontal

5 resolution means that any sub-grid scale events will not be captured and represented by the model, and a finer resolution model may be needed to have better representation of the observations.

4.3 Spring ozone depletion events

4.3.1 Time series

10 Figure 6 shows month-long time series of surface ozone at Tiksi (May 2011), Barrow (March 2010), Summit (April 2010), VRS (April 2010) and Alert (April 2010). Observations are shown as black lines, along with pTOMCAT_SI_OO_VSLS output of surface ozone shown in red and BrO in blue (from the nearest gridbox). Also shown in Fig. 6 are maximum and minimum ozone taken from five adjacent gridboxes in the bottom model layer with the aim of investigating the effect of model resolution on output. From Fig. 6, we see that the p-TOMCAT model can reproduce large ODEs well, e.g., the 1-week-long ODE during

15 7-11 May 2011 at Tiksi and 10-15 March 2010 at Barrow, and the 3-day long ODE during 22-24 April 2010 at VRS. However, the model has a very limited ability to represent small-scale events that last from a few hours to ~1 day. Large discrepancies are found in both timing and magnitude of the ozone depletion. For instance, the one-day long ODE on ~22 April 2010 at Alert is not well captured by the central gridbox closest to the site, i.e., with simulated minimum ozone occurring later by about one day. In general, the central gridbox surface ozone is significantly correlated with observed ozone with high correlation

20 coefficient R of 0.5-0.8 ($p<0.001$) at all sites except Alert where a small $R=0.24$ ($p<0.001$) is obtained (Table 3 column 2).

Figure 6 shows that large ODEs are mostly accompanied by enhanced BrO. Statistical analysis shows that surface BrO simulated is negatively correlated with observed ozone at Tiksi, Summit and VRS with R of -0.49 ($p<0.001$), -0.19 ($p<0.001$) and -0.51 ($p<0.001$) respectively (Table 3 column 3), while at Barrow and Alert, the correlation is not significant (with R of ~-0.05). However, the correlation between observed surface ozone and simulated tropospheric BrO column becomes

25 significant with R of ~-0.2 ($p<0.001$) (Table 3 column 4) at these two sites; a similar phenomenon is seen between observed ozone and GOME-2 BrO_{trop} at Tiksi, Barrow and VRS (Table 3 column 5), though this correlation does not exist at Summit and Alert. In general, boundary layer ozone is influenced by column BrO in the low troposphere rather than by surface BrO, though these two factors are largely correlated in modelling output (Table 3 column 8). For a specific location, surface ozone may not always represent ozone levels in higher layers, so is surface BrO. Therefore, ozonesonde vertical profile data may

30 supply more information than surface data. Note that at extremely low ozone conditions (e.g., after a complete ozone consumption by halogen chemistry in a stable boundary layer), the negative correlation between BrO and ozone concentrations may not exist (Zhao et al., 2016). This is because under that condition, the photochemical equilibrium is shifted from BrO towards atomic Br.

Figure 7 shows time series of tropospheric column BrO from both GOME-2 and pTOMCAT_SI_OO_VSLS run

35 (corresponding to the Fig. 6). The GOME-2 BrO_{trop} data are tropospheric vertical column BrO for each site at the overpass time. In general, p-TOMCAT BrO_{trop} matches GOME-2 BrO_{trop} well with a correlation coefficient $R=0.59$ ($p<0.001$) at Tiksi, 0.37 ($p<0.001$) at Barrow, 0.33 ($p<0.001$) at VRS and 0.30 ($p<0.001$) at Alert. The lowest correlation is seen as Summit with $R=0.16$ ($p<0.1$), where the satellite column does not show significant day-to-day perturbation (Table 3 column 7 or Fig. 7). p-TOMCAT model tends to overestimate satellite column BrO data by factors of 2-3 during BEEs, e.g., during 7-11 May 2011

40 and during 9-15 March 2010, when there are large ODEs observed (Fig. 6a and b, respectively). During non-ODE (or non-BEE) periods, modelled column BrO results are in good agreement with the GOME-2 data.

4.3.2 Vertical profiles

A large ODE observed at Eureka on 3-7 April 2011 has been reported by Zhao et al. (2016), who pointed out that this ODE was a transported event associated with a strong cyclone originating in the Chukchi Sea on 31 March 2011. GOME-2 BrO_{trop} images (Fig. S5) clearly indicated a large spiral BrO plume over the Chukchi Sea on 1 April 2011 (Blechschmidt et al., 2016),

5 which was transported across the Canadian high Arctic in the following days. This event might have influenced both Resolute and Alert, which are located within ~500 km of Eureka. HYSPLIT 6-day back trajectories ending at 12:00 UTC on 5 April 2011 (Fig. 8) show that the air-mass history of the three sites has a very similar transport pattern, further indicating that these three sites were influenced by the same synoptic system. For this reason, we extend this case study by looking at ozonesonde data from all three sites as shown in Fig. 9a-c.

10 We also have the GOME-2 BrO_{trop} overpass time series data (1-10 April 2011) shown in Fig. 10. Ozonesonde data clearly indicate a severe ozone depletion layer at altitude <2 km during 3-7 April 2011 at both Resolute and Eureka, with minimum ozone less than 1 ppbv in the near-surface layer. At Alert, the ozone depletion strength was a bit weaker than at the other two sites, but the depleted ozone layer still reaches an altitude of 1~1.5 km. Moreover, the most severe ozone depletion at Alert on 4 April is not near the surface, but rather at an elevated height of 500-800 m (Fig. 9c). The simulated ozone profiles (Fig. 9d-

15 f) in UKCA_SI_OO_VSLS run generally match the ozonesonde profiles in the 0-4 km range. For this ODE, both the timing of occurrence and height range of the ODE are roughly captured by the model. The modelled BrO profile is shown in Fig.9g-i, with enhanced BrO being simulated in association with ozone depletion. At Eureka, the simulated maximum surface BrO is similar to the MAX-DOAS measurement with a maximum VMR of ~20 pptv for this event (Zhao et al., 2016; 2017). A zoom-in comparison between the GOME-2 tropospheric column BrO and model-integrated BrO for the period of 1-10 April 2011 is

20 shown in Fig. 10. Satellite BrO columns reached a peak firstly on 3 April 2011 at Resolute (Fig. 10a). One day later, the peak appeared at Eureka (Fig. 10b) and Alert (Fig. 10c). The UKCA_SI_OO_VSLS run shows a similar transport pattern of enhanced BrO, which reached Resolute first, and then Eureka and Alert. This finding is consistent with our previous conclusion made in Zhao et al. (2016) that this ODE is transported associated with a large cyclone.

A strong correlation between the UKCA_SI_OO_VSLS BrO_{trop} and the GOME-2 BrO_{trop} data can be seen at Resolute with a

25 high R of 0.71 ($p<0.001$) (Fig. 10d). At the other two sites, the correlation is positive but with small R of ~0.2. The UKCA BrO_{trop} is on average lower than the satellite data by ~50% (refers to the regression equations shown in Fig. 10), which is opposite to the overestimated BrO_{trop} by pTOMCAT model (in Fig. 7). This difference is in line with the above discussed differences in total Br_Y between the two models (in Section 4.1), although the same total bromine emissions are applied.

5 Discussions

30 Regarding tropospheric bromine in the Arctic, as mentioned previously, the uncertainty attributed to model set-ups can be as large as 100% (under the same bromine loading). As a consequence, the ozone loss due to bromine chemistry can be different by a factor of two.

The major factors that affect bromine emissions are SSA production flux and bromine depletion factor used to describe bromine release from SSA. On a global scale, the uncertainty of the sea spray (from open ocean) source can be a factor of four (Lewis

35 and Schwartz, 2004). On sea ice, the blowing snow related SSA production is sensitive to both snow salinity and bulk sublimation flux calculated (as a complex function of near surface wind speed, temperature and relative humidity, etc) (Yang et al., 2019). We lack snow data on Arctic sea ice to constrain the dataset used in this study. For example, a 3.5 times Antarctic Weddell Sea snow salinity is used for the Arctic (Section 3.1). Given that the snow salinity effect on SSA mass production (and on bromine) is almost linear, the uncertainty caused by this factor can be linearly estimated when more snow data in the

40 Arctic are available.

The blowing snow parameters used in this study (including blowing snow particle size distribution, number of SSA formed per saline snow particle, evaporation function involved, etc) mainly affect SSA particle size spectrum rather than mass (Yang et al., 2019), therefore they may only slightly affect both SSA and bromine mass loading when a cut-off size for SSA is applied (a dry NaCl diameter of 10 µm is applied here).

5   Fig. S6 shows ozone from the pTOMCAT_Fixed_DF run, in which a fixed bromine DF scheme (Table S1) is used. For comparison, the pTOMCAT_SI_OO_VSLS run result is shown, in which the seasonal DF scheme (Table 1) is applied. As can be seen, the timing of the spring ozone minimum shifts slightly from April in pTOMCAT_SI_OO_VSLS towards March in pTOMCAT_Fixed_DF, which makes the model agreement poorer, as the observed ozone minimum is in May at the four coastal sites. To achieve better agreement with the observations, the model needs either an even larger seasonal amplitude of

10   bromine DF than that in Table 1 or a further shift of the DF phase by at least one month, e.g., to allow the annual maximum DF (=0.53) to shift from May to June. However, due to lack of year-round SSA bromide data in the Arctic, we could not validate the DF patterns used in this study as this requires systematic measurements of the SSA bromine depletion strength in the Arctic. This is critical as local SSA is a large source of bromine and the seasonal DF not only affects the timing but also affects the total bromine flux to the atmosphere.

15   Also, we simply apply the bromine depletion factor scheme (i.e., Table 1) to both open-ocean-sourced sea spray and sea-ice-sourced SSA. As we know that freshly released sea spray is alkaline with pH>8, and therefore, the anions in sea spray may buffer the absorbed nitrate and sulphate before getting acidified to allow bromide to be released through heterogeneous reaction, e.g., HOBr+Br⁻→Br$_2$ (e.g., Sander et al., 2003; Breider et al., 2009). On sea ice, the situation could be different as surface snow may have been pre-acidified before grains are lifted in to the air to form SSA. Unfortunately, this difference in

20   the process of bromine liberation from SSA particles is beyond the scope of this study, but we note that it could result in bias, e.g., in bromine releasing from air-borne SSA in both timing and locations.

For the first time, using two global chemistry models, we have examined and evaluated various tropospheric bromine sources (bromocarbons, open ocean sea spray and sea-ice-sourced SSA) and their impacts on Arctic boundary layer bromine budget ozone loss. Model experiments clearly reveal that without SI-sourced bromine, models cannot reproduce Arctic ODEs in

25   spring. OO-sourced bromine only affects background atmospheric ozone and cannot by itself produce polar surface ODEs. The modelled tropospheric column of BrO generally matches the GOME-2 satellite data well during non-ODEs (or non-BEEs); during ODEs (or BEEs), modelled BrO$_{trop}$ agrees with satellite data within ~50% in UKCA model and by factors of 2-3 in the p-TOMCAT model. Although our models are not able to reproduce ODEs at all spatial scales, the success of the models in capturing ODEs and BEEs (e.g., at a spatial scale >~500 km) gives additional evidence for the proposed mechanism of SSA

30   production (as well as acting as a source of bromine) from blowing snow on sea ice (Yang et al., 2008; 2019). Therefore, we may predict that changes in sea ice extent and type in a warming climate will influence Arctic boundary layer chemistry and Arctic climate, including the deposition of atmospheric mercury to the surface (Wang et al., 2019).

Author Contributions

XY designed the study, performed model experiments, and interpreted model output. AM provided surface ozone data, and

35   DT provided ozonesonde data of the three Canadian sites. KB, KS and XZ provided MAX-DOAS BrO data at Eureka, AMB and AR provided GOME-2 tropospheric BrO columns, and XZ contributed to GOME-2 and ozonesonde data analysis. XY prepared the manuscript draft with contributions from all co-authors in both data interpretation and discussions.

Acknowledgements

We thank the IASOA group for stimulating and encouraging this investigation. We thank the many observers who obtained these data over many years of careful work. Ozone sounding data and surface data for Alert were provided by Environment and Climate Change Canada (ECCC). DANCEA is acknowledged for the financial support to carry out ozone measurements

5   at Villum Research Station. The Eureka MAX-DOAS BrO measurements were made at the Polar Environment Atmospheric Research Laboratory (PEARL) by the Canadian Network for the Detection of Atmospheric Change (CANDAC), primarily supported by NSERC, CSA, and ECCC. AB and AR gratefully acknowledge the funding by the Deutsche Forschungsgemeinschaft (DFG, German Research Foundation)-Projektnummer 268020496-TRR 172, within the Transregional Collaborative Research Center "ArctiC Amplification: Climate Relevant Atmospheric and SurfaCe Processes,

10   and Feedback Mechanisms (AC)³" in subproject C03. The authors gratefully acknowledge the NOAA Air Resources Laboratory (ARL) for the provision of the HYSPLIT transport and dispersion model and/or READY website (http://www.ready.noaa.gov) used in this publication.

References

Abbatt, J. P. D., Thomas, J. L., Abrahamsson, K., Boxe, C., Granfors, A., Jones, A. E., King, M. D., Saiz-Lopez, A., Shepson,

15   P. B., Sodeau, J., Toohey, D. W., Toubin, C., von Glasow, R., Wren, S. N., and Yang, X.: Halogen activation via interactions with environmental ice and snow in the polar lower troposphere and other regions, Atmos. Chem. Phys., 12, 6237-6271, https://doi.org/10.5194/acp-12-6237-2012, 2012.

Afe, O. T., Richter, A., Sierk, B., Wittrock, F., and Burrows, J. P.: BrO emission from volcanoes: A survey using GOME and SCIAMACHY measurements, Geophys. Res. Lett., 31, L24113, doi:10.1029/2004GL020994, 2004.

20   Ancellet, G., N. Daskalakis, J.C. Raut, D. Tarasick, J. Hair, B. Quennehen, F. Ravetta, H. Schlager, A.J. Weinheimer, A.M. Thompson, B. Johnson, J.L. Thomas, and K.S. Law (2016), Analysis of the latitudinal variability of tropospheric ozone in the Arctic using the large number of aircraft and ozonesonde observations in early summer 2008, Atmos. Chem. Phys., 16, 13341-13358, https://doi:10.5194/acp-16-13341-2016.

Ayers, G. P., Gillett, R. W., Cainey, J. M., and Dick, A. L.: Chloride and bromide loss from sea-salt particles in Southern

25   Ocean air, J. Atmos. Chem., 33, 299– 319, 1999.

Barrie, L. A., J. W. Bottenheim, R. C. Schnell, P. J. Crutzen, and R. A. Rasmussen (1988), Ozone destruction and photochemical reactions at polar in the lower Arctic atmosphere, Nature, 334, 138– 141.

Barrie, L. A., Bottenheim, J. W., Schnell, R. C., Crutzen, P. J., and Rasmussen, R. A.: Ozone destruction and photochemical reactions at polar sunrise in the lower Arctic atmosphere, Nature, 334, 138–141, https://doi.org/10.1038/334138a0, 1988.

30   Begoin, M., Richter, A., Weber, M., Kaleschke, L., Tian-Kunze,X., Stohl, A., Theys, N., and Burrows, J. P.: Satellite observations of long range transport of a large BrO plume in the Arctic,Atmos. Chem. Phys., 10, 6515–6526,doi:10.5194/acp-10-6515-2010, 2010.

Blechschmidt, A.-M., Richter, A., Burrows, J. P., Kaleschke, L., Strong, K., Theys, N., Weber, M., Zhao, X., and Zien, A.: An exemplary case of a bromine explosion event linked to cyclone development in the Arctic, *Atmos. Chem. Phys.*,**16**, 1773-1788,

35   doi:10.5194/acp-16-1773-2016, 2016.

Bottenheim, J. W., Gallant, A. G. & Brice, K. A.: Measurements of NO_y species and O_3 at 82°N latitude, *Geophys. Res. Lett.* 13, 113–116 (1986).

Bottenheim, J.W., J.D. Fuentes, D.W. Tarasick and K.G. Anlauf (2002), Ozone in the Arctic lower troposphere during winter and spring 2000 (ALERT2000), Atmospheric Environment, 36, 2535-2544.

40   Bottenheim, J. W., and E. Chan (2006), A trajectory study into the origin of spring time Arctic boundary layer ozone depletion, *J. Geophys. Res.*, 111, D19301, doi:10.1029/2006JD007055.

Bottenheim, J. W., Netcheva, S., Morin, S., and Nghiem, S. V.: Ozone in the boundary layer air over the Arctic Ocean: measurements during the TARA transpolar drift 2006–2008, Atmos. Chem. Phys., 9, 4545-4557, https://doi.org/10.5194/acp-9-4545-2009, 2009.Braesicke, P., Keeble, J., Yang, X., Stiller, G., Kellmann, S., Abraham, N. L., Archibald, A., Telford, P., and Pyle, J. A.: Circulation anomalies in the Southern Hemisphere and ozone changes, Atmos. Chem. Phys., 13, 10677– 10688,

5   https://doi:10.5194/acp-13-10677-2013, 2013.

Banerjee, A., Archibald, A. T., Maycock, A., Telford, P., Abraham, N. L., Yang, X., Braesicke, P., and Pyle, J.: Lightning NO$_x$, a key chemistry–climate interaction: impacts of future climate change and consequences for tropospheric oxidising capacity, Atmos. Chem. Phys., 14, 9871-9881, https://doi.org/10.5194/acp-14-9871-2014, 2014.

Breider, T., Chipperfield, M. P., Richards, N. A. D., Carslaw, K. S., Mann, G. W., and Spracklen, D. V.: The impact of BrO

10   on dimethylsulfide in the remote marine boundary layer, Geophys. Res. Lett., 37, L02807, doi:10.1029/2009GL040868, 2009.

Buys, Z., Brough, N., Huey, G., Tanner, D., von Glasow, R., andJones, A. E.: Br2, BrCl, BrO and surface ozone in coastal Antarc-tica: a meteorological and chemical analysis, Atmos. Chem.Phys. Discuss., 12, 11035–11077,doi:10.5194/acpd-12-11035-2012, 2012.

Callies, J., Corpaccioli, E., Eisinger, M., Hahne, A., and Lefebvre,A.: GOME-2 – Metop's Second-Generation Sensor for

15   Oper-ational Ozone Monitoring, ESA Bull.-Eur. Space, 102, 28–36,2000.

Cavalieri, D. J., and C. L. Parkinson (2012), Arctic sea ice variability and trends, 1979–2010, *Cryosphere*, 6(4), 881– 889, doi:10.5194/tc-6-881-2012.

de Caritat, P., Hall, G., G`ıslason, S., Belsey, W., Braun, M., Goloubeva, N. I., Olsen, H. K., Scheie, J. O., and Vaive, J. E.: Chemical composition of arctic snow: concentration levels and regional distribution of major elements, Sci. Total Environ.,

20   336, 183–199, doi:10.1016/j.scitotenv.2004.05.031, 2005.

Cao, L. and Gutheil, E.: Numerical simulation of tropospheric ozone depletion in the polar spring, Air Qual. Atmos. Health, 6, 673–686,doi:10.1007/s11869-013-0208-9, 2013

Cao, L., Platt, U., and Gutheil, E.: Role of the boundary layer in the occurrence and termination of the tropospheric ozone depletion events in polar spring, Atmos. Environ., 132, 98–110, doi:http://dx.doi.org/10.1016/j.atmosenv.2016.02.034, 2016.

25   Choi, S., N. Theys, R.J. Salawitch, P.A. Wales, J. Joiner, T.P. Canty, et al.: Link between arctic tropospheric BrO explosion observed from space and sea-salt aerosols from blowing snow investigated using ozone monitoring instrument BrO data and GEOS-5 data assimilation system, J. Geophys. Res. Atmos, 123 (13) (2018), pp. 6954-6983, 10.1029/2017JD026889.

Production flux of sea spray aerosol, Rev. Geophys., 49, RG2001, https://doi.org/10.1029/2010RG000349, 2018.

Choi, S., Wang, Y., Salawitch, R. J., Canty, T., Joiner, J., Zeng, T., Kurosu, T. P., Chance, K., Richter, A., Huey, L. G., Liao,

30   J., Neuman, J. A., Nowak, J. B., Dibb, J. E., Weinheimer, A. J., Diskin, G., Ryerson, T. B., da Silva, A., Curry, J., Kinnison, D., Tilmes, S., and Levelt, P. F.: Analysis of satellite-derived Arctic tropospheric BrO columns in conjunction with aircraft measurements during ARCTAS and ARCPAC, Atmos. Chem. Phys., 12, 1255–1285, https://doi.org/10.5194/acp-12-1255-2012, 2012.

Dee, D. P., Uppala, S. M., Simmons, A. J., Berrisford, P., Poli, P., Kobayashi, S., Andrae, U., Balmaseda, M. A., Balsamo,

35   G., Bauer, P., Bechtold, P., Beljaars, A. C. M., van de Berg, L., Bidlot, J., Bormann, N., Delsol, C., Dragani, R., Fuentes, M., Geer, A. J., Haimberger, L., Healy, S. B., Hersbach, H., Hólm, E. V., Isaksen, L., Kållberg, P., Köhler, M., Matricardi, M., McNally, A. P., Monge-Sanz, B. M., Morcrette, J. J., Park, B. K., Peubey, C., de Rosnay, P., Tavolato, C., Thépaut, J. N., and Vitart, F.: The ERA-Interim reanalysis: configuration and performance of the data assimilation system, Q. J. Roy. Meteor. Soc., 137, 553-597, doi:10.1002/qj.828, 2011.

40   Derwent, RG, Parrish, DD, Galbally, IE, Stevenson, DS, Doherty, RM, et al. (2016): Interhemispheric differences in seasonal cycles of tropospheric ozone in the marine boundary layer: Observation – model comparisons. J Geophys Res. DOI: https://doi.org/10.1002/2016JD024836.

Errera, Q., Daerden, F., Chabrillat, S., Lambert, J. C., Lahoz, W. A.,Viscardy, S., Bonjean, S., and Fonteyn, D.: 4D-Var assimilation of MIPAS chemical observations: ozone and nitrogen dioxide analyses, Atmos. Chem. Phys., 8, 6169–6187, doi:10.5194/acp-8-6169-2008, 2008.

Evans, M. J., Jacob, D. J., Atlas, E., Cantrell, C. A., Eisele, F., Flocke, F., Fried, A., Mauldin, R. L., Ridley, B. A., Wert, B.,
5 Talbot, R.,Blake, D., Heikes, B., Snow, J., Walega, J., Weinheimer, A. J., and Dibb, J.: Coupled evolution of BrOx-ClOx-HOx-NOxchemistry duringbromine-catalyzed ozone depletion events in the arctic boundary layer, J. Geophys. Res. Atmos., 108, doi:10.1029/2002JD002732, 2003.

Falk, S., Sinnhuber, B.-M. (2018). Polar boundary layer bromine explosion and ozone depletion events in the chemistry-climate model EMAC v2.52: Implementation and evaluation of AirSnow algorithm. *Geoscientific Model Development*, 1115–
10 1131.

Fan, S. M., and D. J. Jacob D. J.: Surface ozone depletion in Arctic spring sustained by bromine reactions on aerosols, Nature, 359, 522– 524, 1992.

Frey, M. M., Norris, S. J., Brooks, I. M., Anderson, P. S., Nishimura, K., Yang, X., Jones, A., Nerentorp Mastromonaco, M. G., Jones, D. H., and Wolff, E. W.: First direct observation of sea salt aerosol production from blowing snow above sea ice,
15 Atmos. Chem. Phys. Disc., acp-2019-259, 2019.

Frieß, U., Sihler, H., Sander, R., Pöhler, D., Yilmaz, S., andPlatt, U.: The vertical distribution of BrO and aerosols in theArctic: Measurements by active and passive differential opti-cal absorption spectroscopy, J. Geophys. Res., 116, D00R04,doi:10.1029/2011JD015938, 2011.

Galbally, I.E., Schultz, M.G., Buchmann, B., Gilge, S., Guenther, F., Koide, H., Oltmans, S., Patrick, L., Scheel, H.-E., Smit,
20 H., Steinbacher, M., Steinbrecht, W., Tarasova, O., Viallon, J., Volz-Thomas, A., Weber, M., Wielgosz R. and Zellweger C. (2013) Guidelines for Continuous Measurement of Ozone in the Troposphere, GAW Report No 209, Publication WMO-No. 1110, ISBN 978-92-63-11110-4, World Meteorological Organisation, Geneva Switzerland, 76 pp. http://www.wmo.int/pages/prog/arep/gaw/gaw-reports.html

Ganzeveld, L. and Lelieveld, J.: Dry deposition parametisation in achemistry general circulation model and its influence on
25 the dis-tribution of reactive trace gases, J. Geophys. Res., 100, 20999–21012, doi:10.1029/95JD02266, 1995.

Giannakopoulos, C.: Modelling the impact of physical and removalprocesses on tropospheric chemistry, Ph.D. thesis, University ofCambridge, 1998.

Gaudel, A. and Cooper, O. R.: Tropospheric Ozone Assessment Re-port: Present-day distribution and trends of tropospheric ozonerelevant to climate and global atmospheric chemistry model eval-uation, Elem. Sci. Anth., in press, 2018.

30 Hatakka, J., Aalto, T., Aaltonen, V., Aurela, M., Hakola, H., Komp-pula, M., Laurela, T., Lihavainen, H., Paatero, J., Salminen, K.,and Viisanen, Y.: Overview of the atmospheric research activi-ties and results at Pallas GAW station, Boreal Environ. Res., 8,365–383, 2003.

Hardacre, C., Wild, O., and Emberson, L.: An evaluation of ozonedry deposition in global scale chemistry climate models, At-mos. Chem. Phys., 15, 6419–6436, https://doi.org/10.5194/acp-15-6419-2015, 2015.

35 Helmig, D., Oltmans, S. J., Carlson, D., Lamarque, J.-F., Jones,A., Labuschagne, C., Anlauf, K., and Hayden, K.: A Review of surface ozone in the polar regions, Atmos. Environ., 41(24),5138–5161, 2007.

He, H., D.W. Tarasick, W.K. Hocking, T.K. Carey-Smith, Y. Rochon, J. Zhang, P.A. Makar, M. Osman, J. Brook, M. Moran, D. Jones, C. Mihele, J.C. Wei, G. Osterman, P.S. Argall, J. McConnell and M.S. Bourqui (2011), Transport Analysis of Ozone Enhancement in Southern Ontario during BAQS-Met, Atmos. Chem. Phys., 11, 2569-2583, doi:10.5194/ acp-11-2569-2011.

40 Helmig, D., Oltmans, S. J., Morse, T. O., and Dibb, J. E.: What is causing high ozone at Summit, Greenland?, Atmos. Environ.,41(24), 5031–5043, https://doi.org/10.1016/j.atmosenv.2006.05.084, 2007.

Holtslag, A. A. M., and Boville, B. A.: Local versus non-local boundary layer diffusion in a global climate model, J. Clim., 6, 1825-1842, https://doi.org/10.1175/1520-0442(1993)006<1825:LVNBLD>2.0.CO;2, 1993.

Honrath, R. E., M. C. Peterson, S. Guo, J. E. Dibb, P. B. Shepson, *and* B. Campbell *(*1999*),* Evidence of NO$_x$ production within or upon ice particles in the Greenland snowpack, Geophys. Res. Lett., 26, 695–698, *doi:*10.1029/1999GL900077.

Hoyle, C. R., Maréchal, V., Russo, M. R., Allen, G., Arteta, J., Chemel, C., Chipperfield, M. P., D'Amato, F., Dessens, O., Feng, W., Hamilton, J. F., Harris, N. R. P., Hosking, J. S., Lewis, A. C., Morgenstern, O., Peter, T., Pyle, J. A., Reddmann, T., Richards, N. A. D., Telford, P. J., Tian, W., Viciani, S., Volz-Thomas, A., Wild, O., Yang, X., and Zeng, G.: Representation of tropical deep convection in atmospheric models – Part 2: Tracer transport, Atmos. Chem. Phys., 11, 8103-8131, https://doi.org/10.5194/acp-11-8103-2011, 2011.

Huang, J., & Jaeglé, L. (2017). Wintertime enhancements of sea salt aerosol in polar regions consistent with a sea ice source from blowing snow. *Atmospheric Chem. Phys.*, *17*(5), 3699–3712. https://doi.org/10.5194/acp-17-3699-2017.Jacobi, H.-W., Morin, S., and Bottenheim, J. W.: Observation of widespread depletion of ozone in the springtime boundary layer of the central Arctic linked to mesoscale synoptic conditions, J. Geophys. Res., 115, D17302, doi:10.1029/2010JD013940, 2010.

Jaeglé, L., Quinn, P. K., Bates, T. S., Alexander, B., and Lin, J.-T.: Global distribution of sea salt aerosols: new constraints from in situ and remote sensing observations, Atmos. Chem. Phys., 11, 3137-3157, doi:10.5194/acp-11-3137-2011, 2011.

Johnson, C., Mann, G., Bellouin, N., and D Jacobi, H.-W., Morin, S., and Bottenheim, J. W.: Observation of widespread depletion of ozone in the springtime boundary layer of the central Arctic linked to mesoscale synoptic conditions, J. Geophys. Res., 115, D17302, doi:10.1029/2010JD013940, 2010.

Kaleschke, L., Richter, A., Burrows, J., Afe, O., Heygster, G.,Notholt, J., Rankin, A. M., Roscoe, H. K., Hollwedel, J., Wagner, T., and Jacobi, H.-W.: Frost flowers on sea ice as a sourceof sea salt and their influence on tropospheric halogen chemistry, Geophys. Res. Lett., 31, L16114, doi:10.1029/2004GL020655,2004.

Kerr, J.B., H. Fast, C.T. McElroy, S.J. Oltmans, J.A. Lathrop, E. Kyro, A. Paukkunen, H. Claude, U. Köhler, C.R. Sreedharan, T. Takao and Y. Tsukagoshi (1994), The 1991 WMO international ozonesonde intercomparison at Vanscoy, Canada, Atmosphere-Ocean, 32, 685-716.

Komhyr, W.D. (1969), Electrochemical concentration cells for gas analysis, Ann. Geoph., 25, 203-210.

Kwok, R., and D.A. Rothrock. 2009. Decline in Arctic sea ice thickness from submarine and ICESat records: 1958-2008. *Geophysical Research Letters* 36: L15501.

Laurila, T., Observational study of transport and photochemical formation of ozone over northern Europe, *J. Geophys. Res.*, 104, 26,235– 26,243, 1999.

Law, K. S., P.-H. Plantevin, D. E. Shallcross, H. Rogers, C. Grouhel, V. Thouret, A. Marenco, and J. A. Pyle (1998), Evaluation of modelled O3 using MOZAIC data, J. Geophys. Res., 103, 25,721– 25,740.

Law, K. S., Plantevin, P. -H., Thouret, V., Marenco, A., Asman, W. A. H., Lawrence, M.,25Crutzen P. J., M¨uller, J. -F., Hauglustaine, D. A., and Kanakidou, M.: Comparison betweenglobal chemistry transport model results and Measurement of Ozone by Airbus In-ServiceAircraft (MOZAIC) data, J. Geophys. Res., 105, 1503–1525, 2000.

Law, K. S., and Stohl A.: Arctic air pollution: Origins and impacts, Science, 315, 1537–1540, 2007.

Laxon, S. W., et al. (2013), CryoSat estimates of Arctic sea ice volume, *Geophys. Res. Lett.*, 40, doi:10.1002/grl.50193.

Legrand, M., Yang, X., Preunkert, S., and Theys, N.: Year-roundrecords of sea salt, gaseous, and particulate inorganic brominein the atmospheric boundary layer at coastal (Dumont d'Urville) and central (Concordia) East Antarctic sites, J. Geophys. Res.-Atmos., 121,997–1023, doi:10.1002/2015JD024066, 2016.

Levine, J. G., Yang, X., Jones, A. E., and Wolff, E. W.: Sea salt as an ice core proxy for past sea ice extent: A process-based model study, J. Geophys. Res. Atmos., 119, 5737–5756, doi:10.1002/2013JD020925, 2014.

Liao, J., Sihler, H., Huey, L. G., Neuman, J. A., Tanner, D. J., Frieß,U., Platt, U., Flocke, F. M., Orlando, J. J., Shepson, P. B., Beine,H. J., Weinheimer, A. J., Sjostedt, S. J., Nowak, J. B., Knapp, D. J., Staebler, R. M., Zheng, W., Sander, R., Hall, S. R., and Ull-mann, K.: A comparison of Arctic BrO measurements by chem-ical ionization mass spectrometry and long path-differential op-tical absorption spectroscopy, J. Geophys. Res., 116, D00R02,doi:10.1029/2010JD014788, 2011.

Liao, J., Huey, L. G., Tanner, D. J., Flocke, F. M., Orlando,J. J., Neuman, J. A., Nowak, J. B., Weinheimer, A. J., Hall,S. R., Smith, J. N., Fried, A., Staebler, R. M., Wang, Y.,Koo, J.-H., Cantrell, C. A., Weibring, P., Walega, J., Knapp,D. J., Shepson, P. B., and Stephens, C. R.: Observations ofinorganic bromine (HOBr, BrO, and Br2) speciation at Bar-row, Alaska, in spring 2009, J. Geophys. Res., 117, D00R16,doi:10.1029/2011JD016641, 2012.

5   Lindsay, R.W., and J. Zhang. 2005. The thinning of Arctic sea ice, 1988-2003: Have we passed a tipping point? *Journal of Climate* 18: 4879-4894.

Liu, G., J.J. Liu, D.W. Tarasick, V.E. Fioletov, J.J. Jin, O. Moeni, X. Liu, C.E. Sioris, M. Osman: A global tropospheric ozone climatology from trajectory-mapped ozone soundings, Atmos. Chem. Phys., 13 (2013), 10659-10675, 10.5194/acp-13-10659-2013.

10   Luhar, A. K., Woodhouse, M. T., and Galbally, I. E.: A revised global ozone dry deposition estimate based on a new two-layer parameterisation for air–sea exchange and the multi-year MACC composition reanalysis, Atmos. Chem. Phys., 18, 4329-4348, https://doi.org/10.5194/acp-18-4329-2018, 2018.

Michalowski, B. A., J. S. Francisco, S. M. Li, L. A. Barrie, J. W. Bottenheim, and P. B. Shepson (2000), A computer model study of multiphase chemistry in the Arctic boundary layer during polar sunrise, *J. Geophys. Res.*, 105, 15,131– 15,145.

15   Monks, P. S..: A review of the observations and origins of the spring ozone maximum, Atmospheric Environment, 34, 3545-3561, https://doi.org/10.1016/S1352-2310(00)00129-1, 2000.

Morgenstern, O., Braesicke, P., O'Connor, F. M., Bushell, A. C., Johnson, C. E., Osprey, S. M., and Pyle, J. A.: Evaluation of the new UKCA climate-composition model – Part 1: The stratosphere, Geosci. Model Dev., 2, 43–57, doi:10.5194/gmd-2-43-2009, 2009.

20   Olonscheck, D., T. Mauritsen, and Notz D.: Arctic sea-ice variability is primarily driven by atmospheric temperature fluctuations. *Nature Geoscience*. doi:10.1038/s41561-019-0363-1, 2019.

Oltmans, S.J., A.S. Lefohn, J.M. Harris, D.W. Tarasick, A.M. Thompson, H. Wernli, B.J. Johnson, P.C. Novelli, S.A. Montzka, J.D. Ray, L.C. Patrick, C. Sweeney, A. Jefferson, T. Dann, J. Davies, M. Shapiro and B.N. Holben (2010), Enhanced ozone over western North America from biomass burning in Eurasia during April 2008 as seen in surface and

25   profile observations, Atmospheric Environment, 44, (35) 4497-4509, ISSN 1352-2310, doi: 10.1016/j.atmosenv.2010.07.004.

O'Connor, F., Carver, G., Savage, N., Pyle, J., Methven, J., Arnold, S., Dewey, K., and Kent, J.: Comparison and visualisation of high-resolution transport modelling with aircraft measurements, Atmos. Sci. Lett., 6, 164-170, 2005.

O'Dowd, C. D., Smith, M. H., Consterdine, I. E., and Lowe, J. A.: Marine aerosol, sea salt, and the marine sulphur cycle: A

30   short review, Atmos. Environ., 31, 73–80, 1997.

O'Dowd, C. D., Lowe, J., Smith, M. H., and Kaye, A. D.: The relative importance of sea-salt and nss-sulphate aerosol to the marine CCN population: An improved multi-component aerosol-droplet parameterisation, Q. J. R. Meteorol. Soc, 125 (556 Part B), 1295–1313, 1999.

Parrella, J. P., Jacob, D. J., Liang, Q., Zhang, Y., Mickley, L. J., Miller, B., Evans, M. J., Yang, X., Pyle, J. A., Theys, N., and

35   Van Roozendael, M.: Tropospheric bromine chemistry: implications for present and pre-industrial ozone and mercury, Atmos. Chem. Phys., 12, 6723-6740, https://doi.org/10.5194/acp-12-6723-2012, 2012.

Parrish, DD, Galbally, IE, Lamarque, JF, Naik, V, Horowitz, L, et al. 2016 Seasonal cycles of O3 in the marine boundary layer: Observation and model simulation comparisons. J Geophys Res 121(1): 538–557. DOI: https://doi.org/10.1002/2015JD024101.Quinn, P. K., Miller, T. L., Bates, T. S., Ogren, J. A., Andrews, E., and Shaw, G. E.: A 3-year

40   record of simultaneously measured aerosol chemical and optical properties at Barrow Alaska, J. Geophys. Res., 107(D11), 4130, doi:10.1029/2001JD001248, 2002.

Quinn, P. K., Bates, T. S., Baum, E., Doubleday, N., Fiore, A. M., Flanner, M., Fridlind, A., Garrett, T. J., Koch, D., Menon, S., Shindell, D., Stohl, A., and Warren, S. G.: Short-lived pollutants in the Arctic: their climate impact and possible mitigation strategies, Atmos. Chem. Phys., 8, 1723-1735, https://doi.org/10.5194/acp-8-1723-2008, 2008.

Pratt, K. A., Custard, K. D., Shepson, P. B., Douglas, T. A., Pöhler, D., General, S., Zielcke, J., Simpson, W. R., Platt, U.,

5 Tanner, D. J., Huey, L. G., Carlsen, M., and Stirm, B. H.: Photochemical production of molecular bromine in Arctic surface snowpacks, Nat. Geosci., 6, 351–356, https://doi.org/10.1038/NGEO1779, 2013.

Reader, M. C., and McFarlane, N.: Sea-salt aerosol distribution during the Last Glacial Maximum and its implications for mineral dust, J. Geophys. Res., 108(D8), 4253, doi:10.1029/2002JD002063, 2003.

Rayner, N. A., et al. (2003), Global analyses of sea surface temperature, sea ice, and night marine air temperature since the

10 late nineteenth century, J. Geophys. Res., 108(D14), 4407, doi:10.1029/2002JD002670.

Rhodes, R. H., Yang, X., Wolff, E. W., McConnell, J. R., and Frey, M. M.: Sea ice as a source of sea salt aerosol to Greenland ice cores: a model-based study, Atmos. Chem. Phys., 17, 9417-9433, https://doi.org/10.5194/acp-17-9417-2017, 2017.

Rolph, G., Stein, A., and Stunder, B., (2017). Real-time Environmental Applications and Display sYstem: READY. Environmental Modelling & Software, 95, 210-228, https://doi.org/10.1016/j.envsoft.2017.06.025.

15 Russo, M. R., V. Marecal, C. R. Hoyle, J. Arteta, C. Chemel, O. Dessens, W. Feng, J. S. Hosking, P. Telford, O. Wild, X. Theys, N., M. Van Roozendael, F. Hendrick, X. Yang, I. De Smedt, A. Richter, M. Begoin, Q. Errera, P. V. Johnston, K. Kreher, and M. De Mazière, Global observations of tropospheric BrO columns using GOME-2 satellite data, *Atmos. Chem. Phys.*, 11, 1791-1811, doi:10.5194/acp-11-1791-2011, 2011.

Saiz-Lopez, A., Plane, J. M. C., Mahajan, A. S., Anderson, P. S.,Bauguitte, S. J.-B., Jones, A. E., Roscoe, H. K., Salmon, R.

20 A., Bloss, W. J., Lee, J. D., and Heard, D. E.: On the vertical distri-bution of boundary layer halogens over coastal Antarctica: im-plications for O3, HOx, NOxand the Hg lifetime, Atmos. Chem.Phys., 8, 887–900,doi:10.5194/acp-8-887-2008, 2008.

Salawitch, R., Canty, T., Kurosu, T., Chance, K., Liang, Q., daSilva, A., Pawson, S., Nielsen, J. E., Rodriguez, J. M., Bhartia, P. K., Liu, X., Huey, L. G., Liao, J., Stickel, R. E., Tanner, DJ., Dibb, J. E., Simpson, W. R., Donohoue, D., Weinheimer, A.,Flocke, F., Knapp, D., Montzka, D., Neuman, J. A., Nowak, J.B., Ryerson, T. B., Oltmans, S., Blake, D. R., Atlas, E. L.,

25 Kinni-son, D. E., Tilmes, S., Pan, L. L., Hendrick, F., Van Roozendael.,M., Kreher, K., Johnston, P. V., Gao, R. S., Johnson, B., Bui, T.P., Chen, G., Pierce, R. B., Crawford, J. H., and Jacob, D. J.:A new interpretation of total column BrO during Arctic spring,Geophys. Res. Lett., 37, L21805,doi:10.1029/2010GL043798,2010.

Sander, R., Keene, W. C., Pszenny, A. A. P., Arimoto, R., Ayers, G. P., Baboukas, E., Cainey, J. M., Crutzen, P. J., Duce, R. A., Hönninger, G., Huebert, B. J., Maenhaut, W., Mihalopoulos, N., Turekian, V. C., and Van Dingenen, R.: Inorganic bromine

30 in the marine boundary layer: a critical review, Atmos. Chem. Phys., 3, 1301-1336, https://doi.org/10.5194/acp-3-1301-2003, 2003.

Schultz, M.G., Schröder, S., Lyapina, O., Cooper, O., Galbally, I., Petropavlovskikh, I., von Schneidemesser, E., Tanimoto, H., Elshorbany, Y., Naja, M., Seguel, R., Dauert, U., Eckhardt, P., Feigenspahn, S., Fiebig, M., Hjellbrekke, A.-G., Hong, Y.-D., Christian Kjeld, P., Koide, H., Lear, G., Tarasick, D., Ueno, M., Wallasch, M., Baumgardner, D., Chuang, M.-T., Gillett,

35 R., Lee, M., Molloy, S., Moolla, R., Wang, T., Sharps, K., Adame, J.A., Ancellet, G., Apadula, F., Artaxo, P., Barlasina, M., Bogucka, M., Bonasoni, P., Chang, L., Colomb, A., Cuevas, E., Cupeiro, M., Degorska, A., Ding, A., Fröhlich, M., Frolova, M., Gadhavi, H., Gheusi, F., Gilge, S., Gonzalez, M.Y., Gros, V., Hamad, S.H., Helmig, D., Henriques, D., Hermansen, O., Holla, R., Huber, J., Im, U., Jaffe, D.A., Komala, N., Kubistin, D., Lam, K.-S., Laurila, T., Lee, H., Levy, I., Mazzoleni, C., Mazzoleni, L., McClure-Begley, A., Mohamad, M., Murovic, M., Navarro-Comas, M., Nicodim, F., Parrish, D., Read, K.A.,

40 Reid, N., Ries, L., Saxena, P., Schwab, J.J., Scorgie, Y., Senik, I., Simmonds, P., Sinha, V., Skorokhod, A., Spain, G., Spangl, W., Spoor, R., Springston, S.R., Steer, K., Steinbacher, M., Suharguniyawan, E., Torre, P., Trickl, T., Weili, L., Weller, R., Xu, X., Xue, L. and Zhiqiang, M., 2017. Tropospheric Ozone Assessment Report: Database and Metrics Data of Global Surface Ozone Observations. *Elem Sci Anth*, 5, p.58. DOI: http://doi.org/10.1525/elementa.244.

Seabrook, J. A., Whiteway, J. A., Gray, L. H., Staebler, R., and Herber, A.: Airborne lidar measurements of surface ozone depletion over Arctic sea ice, Atmos. Chem. Phys., 13, 6023-6029, https://doi.org/10.5194/acp-13-6023-2013, 2013.

Simpson, W. R., von Glasow, R., Riedel, K., Anderson, P., Ariya, P., Bottenheim, J., Burrows, J., Carpenter, L. J., Frieß, U., Goodsite, M. E., Heard, D., Hutterli, M., Jacobi, H.-W., Kaleschke, L., Neff, B., Plane, J., Platt, U., Richter, A., Roscoe, H.,
5   Sander, R., Shepson, P., Sodeau, J., Steffen, A., Wagner, T., and Wolff, E.: Halogens and their role in polar boundary-layer ozone depletion, Atmos. Chem. Phys., 7, 4375-4418, https://doi.org/10.5194/acp-7-4375-2007, 2007a.

Simpson, WR, Carlson, D, Hönninger, G, Douglas, TA, Sturm, M, Perovich, D and Platt, U.: First-year sea-ice contact predicts bromine monoxide (BrO) levels at Barrow, Alaska better than potential frost flower contact. *Atmospheric Chemistry and Physics* **7**(3): 621–627. ISSN 1680-7324. http://www.atmos-chem-phys.net/7/621/2007/. DOI: 10.5194/acp-7-621-2007,
10   2007b.

Skov, H. Christensen, J. Goodsite, M.E. Heidam, N.Z. Jensen, B. Wåhlin, P. and Geernaert, G.: The fate of elemental mercury in Arctic during atmospheric mercury depletion episodes and the load of atmospheric mercury to Arctic. ES & T, 38, 2373-2382, 2004.

Skov, H. Hjorth J. Nordstrøm, C. Jensen, B. Christoffersen, C. Poulsen, M.B. Liisberg, J.B. and Dall'Osto M.: The variability
15   of ozone and mercury at Villum Research Station, Station Nord in North Greenland from 1995 to 2017. (Ready for submission Aug. 2019 for Atm. Env.)

Smit H.G.J and D. Kley (1998), JOSIE: The 1996 WMO International intercomparison of ozonesondes under quasi flight conditions in the environmental simulation chamber at Jülich, WMO Global Atmosphere Watch Report No. 130, WMO TD No. 926, World Meteorological Organization, Geneva.

20   Smit, H.G.J., W. Straeter, B. Johnson, S. Oltmans, J. Davies, D.W. Tarasick, B. Hoegger, R. Stubi, F. Schmidlin, T. Northam, A. Thompson, J. Witte, I. Boyd and F. Posny (2007) Assessment of the performance of ECC-ozonesondes under quasi-flight conditions in the environmental simulation chamber: Insights from the Juelich Ozone Sonde Intercomparison Experiment (JOSIE), J. Geophys Res., 112, D19306, doi:10.1029/2006JD007308.

Stein, A.F., Draxler, R.R, Rolph, G.D., Stunder, B.J.B., Cohen, M.D., and Ngan, F., (2015). NOAA's HYSPLIT atmospheric
25   transport and dispersion modeling system, Bull. Amer. Meteor. Soc., 96, 2059-2077, http://dx.doi.org/10.1175/BAMS-D-14-00110.1.

Tarasick, D.W., H.G.J. Smit, A.M. Thompson, G.A. Morris, J.C. Witte, J. Davies, T. Nakano, R. van Malderen, R.M. Stauffer, T. Deshler, B.J. Johnson, R. Stübi, C. Sterling and S.J. Oltmans (2019c), Improving ECC Ozonesonde Data Quality: Assessment of Current Methods & Outstanding Issues, manuscript to be submitted to BAMS.

30   Tiedtke, M.: A comprehensive mass flux scheme for cumulus parameterization in large scale models, Mon. Weather Rev., 117, 1779–1800, 1989.

Tarasick, D.W., and J.W Bottenheim (2002), Surface ozone depletion episodes in the Arctic and Antarctic from historical ozonesonde records, Atmos. Chem. Phys., 2, 197-205.

Tang, T., and J. C. McConnell, Autocatalytic release of bromine from Arctic snow pack during polar sunrise, Geophys. Res.
35   Lett., 23, 2633- 2636, 1996.

Tarasick, D.W., J. Davies, H.G.J. Smit and S.J. Oltmans (2016), A re-evaluated Canadian ozonesonde record: measurements of the vertical distribution of ozone over Canada from 1966 to 2013, Atmos. Meas. Tech. 9, 195-214, doi:10.5194/amt-9-195-2016.

Tarasick, D.W., I. Galbally, O.R. Cooper, M.G. Schultz, G. Ancellet, T. LeBlanc, T.J. Wallington, J. Ziemke, X. Liu, M.
40   Steinbacher, J. Stähelin, C. Vigouroux, J.W. Hannigan, O. García, G. Foret, P. Zanis, E. Weatherhead, I. Petropavlovskikh, H. Worden, M. Osman, J. Liu, K.-L. Chang, A. Gaudel,M. Lin, M. Granados-Muñoz, A.M. Thompson, S.J. Oltmans, J. Cuesta, G. Dufour, V. Thouret, B. Hassler, T. Trickl and J.L. Neu (2019a), TOAR- Observations: Tropospheric ozone observations from 1877 to 2017, measurement uncertainties and trends., *Elementa: Science of the Anthropocene,* accepted.

Tarasick, D.W., T.K. Carey-Smith, W.K. Hocking, O. Moeini, H. He, J. Liu, M. Osman, A.M. Thompson, B. Johnson, S.J. Oltmans and J.T. Merrill (2019a), Quantifying stratosphere-troposphere transport of ozone using balloon-borne ozonesondes, radar windprofilers and trajectory models, Atmos. Environ., 198 (2019b), 496–509, https://doi.org/10.1016/j.atmosenv.2018.10.040.

5 Thomas, J. L., Stutz, J., Lefer, B., Huey, L. G., Toyota, K., Dibb, J. E., and von Glasow, R.: Modeling chemistry in and above snow at Summit, Greenland – Part 1: Model description and results, Atmos. Chem. Phys., 11, 4899–4914, https://doi.org/10.5194/acp-11-4899-2011, 2011.

Theys, N., Van Roozendael, M., Hendrick, F., Yang, X., De Smedt, I., Richter, A., Begoin, M., Errera, Q., Johnston, P. V., Kreher, K., and De Mazière, M.: Global observations of tropospheric BrO columns using GOME-2 satellite data, Atmos.
10 Chem. Phys., 11, 1791-1811, https://doi.org/10.5194/acp-11-1791-2011, 2011.

Toyota, K., McConnell, J. C., Lupu, A., Neary, L., McLinden, C. A., Richter, A., Kwok, R., Semeniuk, K., Kaminski, J. W., Gong, S. L., Jarosz, J., Chipperfield, M. P., & Sioris, C. E. (2011). Analysis of reactive bromine production and ozone depletion in the Arctic boundary layer using 3-D simulations with GEM-AQ: Inference from synoptic-scale patterns. *Atmospheric Chemistry and Physics*, 11(8), 3949– 3979. https://doi.org/10.5194/acp-11-3949-2011

15 Uttal, T.; Starkweather, S.; Drummond, J. R.; Vihma, T.; Makshtas, A. P.; Darby, L. S.; Burkhart, J. F.; Cox, C. J.; Schmeisser, L. N.; Haiden, T.; Maturilli, M.; Shupe, M. D.; De Boer, G.; Saha, A.; Grachev, A. A.; Crepinsek, S. M.; Bruhwiler, L.; Goodison, B.; McArthur, B.; Walden, V. P.; Dlugokencky, E. J.; Persson, P. O. G.; Lesins, G.; Laurila, T.; Ogren, J. A.; Stone, R.; Long, C. N.; Sharma, S.; Massling, A.; Turner, D. D.; Stanitski, D. M.; Asmi, E.; Aurela, M.; Skov, H.; Eleftheriadis, K.; Virkkula, A.; Platt, A.; Forland, E. J.; Iijima, Y.; Nielsen, I. E.; Bergin, M. H.; Candlish, L.; Zimov, N. S.; Zimov, S. A.;
20 O'Neill, N. T.; Fogal, P. F.; Kivi, R.; Konopleva-Akish, E. A.; Verlinde, J.; Kustov, V. Y.; Vasel, B.; Ivakhov, V. M.; Viisanen, Y.; Intrieri, J. M., International Arctic Systems for Observing the Atmosphere: An International Polar Year Legacy Consortium. Bull. Amer. Meteorol. Soc. 2016, 97 (6), 1033-1056.

Viscardy, S., Errera, Q., Christophe, Y., Chabrillat, S., and Lambert,J.-C.: Evaluation of Ozone Analyses From UARS MLS Assimi-lation by BASCOE Between 1992 and 1997, IEEE J-STARS, 3,190–202, doi:10.1109/JSTARS.2010.2040463, 2010.

25 Vogt, R., Crutzen, P. J., and Sander, R.: A mechanism for halogen release from sea-salt aerosol in the remote marine boundary layer, Nature, 383, 327–330, doi:10.1038/383327a0, 1996.

Voulgarakis, A., Yang, X., and Pyle, J. A.: How different would tropospheric oxidation be over an ice-free Arctic?, Geophys. Res. Lett., 36, L23807, doi:10.1029/2009GL040541, 2009.

Wagner, T., U. Platt: Satellite mapping of enhanced BrO concentrations in the troposphere, Nature, 395 (1998), pp. 486-490.

30 Walker T.W., D.B.A. Jones, M. Parrington,, D.K. Henze, L.T. Murray, J.W. Bottenheim, K. Anlauf, J.R. Worden, K.W. Bowman, C. Shim, K. Singh, M. Kopacz, D.W. Tarasick, J. Davies, P. von der Gathen, A.M. Thompson and C.C. Carouge (2012), Impacts of midlatitude precursor emissions and local photochemistry on ozone abundances in the Arctic, J. Geophys. Res., 117, D01305, doi:10.1029/2011JD016370.

Wang, K. Y., Pyle, J. A., Sandersen, M. G., and Bridgeman, c.: Implimentation of a convective atmospheric boundary layer
35 scheme in a tropospheric chemistry transport model, J. Geophys. Res., 104, 23,729– 23,745, 1999.

Wang, S., S.M. McNamara, C.W. Moore, D. Obrist, A. Steffen, P.B. Shepson, R.M. Staebler, A.R.W. Raso, K.A. Pratt (2019), Direct detection of atmospheric atomic bromine leading to mercury and ozone depletion, Proceedings of the National Academy of Sciences Jul 2019, 116 (29) 14479-14484; DOI: 10.1073/pnas.1900613116.

Warwick, N. J., J. A. Pyle, G. D. Carver, X. Yang, N. H. Savage, F. M. O'Connor, and R. A. Cox, Global modeling of biogenic
40 bromocarbons, *J. Geophys. Res.*, 111, D24305, doi:10.1029/2006JD007264, 2006.

Yang, X., Cox, R. A., Warwick, N. J., Pyle, J. A., Carver, G. D., O'Connor, F. M., and Savage, N.H.: Tropospheric bromine chemistry and its impacts on ozone: A model study. *J. Geophys. Res.*, 110, D23311, doi:10.1029/2005JD006244, 2005.

Yang, X., Pyle, J. A., and Cox, R. A.: Sea salt aerosol production and bromine release: Role of snow on sea ice, Geophys. Res. Lett., 35 (L16815), doi:10.1029/2008gl034536, 2008.

Yang, X., Pyle, J. A., Cox, R. A., Theys, N., and Van Roozendael, M.: Snow-sourced bromine and its implications for polar tropospheric ozone, Atm. Chem. Phys., 10, 7763-7773, doi:10.5194/acp-10-7763-2010, 2010.

5 Yang, X., N. L. Abraham, A. T. Archibald, P. Braesicke, J. Keeble, P. J. Telford, N. J. Warwick, and J. A. Pyle, How sensitive is the recovery of stratospheric ozone to changes in concentrations of very short lived bromocarbons? Atmos. Chem. Phys., 14, 10431-10438, doi:10.5194/acp-14-10431-2014, 2014.

Yang, X., Neděla, V., Runštuk, J., Ondrušková, G., Krausko, J., Vetráková, Ľ., and Heger, D.: Evaporating brine from frost flowers with electron microscopy and implications for atmospheric chemistry and sea-salt aerosol formation, Atmos. Chem.

10 Phys., 17, 6291-6303, https://doi.org/10.5194/acp-17-6291-2017, 2017.

Yang, X., Frey, M. M., Rhodes, R. H., Norris, S. J., Brooks, I. M., Anderson, P. S., Nishimura, K., Jones, A. E., and Wolff, E. W.: Sea salt aerosol production via sublimating wind-blown saline snow particles over sea ice: parameterizations and relevant microphysical mechanisms, Atmos. Chem. Phys., 19, 8407–8424, https://doi.org/10.5194/acp-19-8407-2019, 2019.

Young, PJ, Naik, V, Fiore, AM, Gaudel, A, Guo, J, Lin, MY, Neu, J, Parrish, D, Reider, HE, Schnell, JL, Tilmes, S, Wild, O,

15 Zhang, L, Brandt, J, Delcloo, A, Doherty, RM, Geels, C, Hegglin, M, Hu, L, Im, U, Kumar, R, Luhar, A, Murray, L, Plummer, D, Rodriguez, J, Saiz-Lopez, A, Schultz, MG, Woodhouse, M, Zeng, G & Ziemke, J, 'Tropospheric Ozone Assessment Report: Assessment of global-scale model performance for global and regional ozone distributions, variability, and trends' Elementa: Science of the Anthropocene, vol. 6, no. 1. https://doi.org/10.1525/elementa.265, 2018.

Zhao, X., Strong, K., Adams, C., Schofield, R., Yang, X., Richter, A., Friess, U., Blechschmidt, A.-M., and Koo, J.-H.: A case

20 study of a transported bromine explosion event in the Canadian high arctic, J. Geophys. Res. Atmos., 121, 457–477, doi:10.1002/2015JD023711, 2016.

Zhao, X., Weaver, D., Bognar, K., Manney, G., Millán, L., Yang, X., Eloranta, E., Schneider, M., and Strong, K.: Cyclone-induced surface ozone and HDO depletion in the Arctic, Atmos. Chem. Phys., 17, 14955-14974, https://doi.org/10.5194/acp-17-14955-2017, 2017.

Table 1. Monthly mean SSA bromine depletion factor (DF) scheme applied in the NH (>45°N), which is derived from the data in the Southern Hemisphere at Cape Grim (41°S), Macquarie Island (55°S) and Dumont d'Urville (66°S) (Ayers, 1999, Legrand et al. 2016). Note that a 6-month shift of the phase is applied to match the NH seasons. A cut-off dry NaCl diameter of 10 µm is applied (i.e., DF=0 at diameter > 10 µm).

Month	DF
January	0.175
February	0.260
March	0.445
April	0.500
May	0.530
June	0.383
July	0.225
August	0.168
September	0.192
October	0.170
November	0.145
December	0.07

Table 2. Model experiments with various bromine sources from sea ice (SI), open ocean (OO) and very short-lived substances (VSLS) of bromocarbons. Two bromine depletion factor (DF) schemes are used: with seasonal cycle (Table 1) and without seasonal cycle (i.e., using a fixed DF in Table S1).

Models and Experiments	Bromine from SI	Bromine from OO	Bromine from VSLS	DF for SSA
pTOMCAT_SI_OO_VSLS	Yes	Yes	Yes	Seasonal
pTOMCAT_No_Br	No	No	No	Seasonal
pTOMCAT_VSLS	No	No	Yes	Seasonal
pTOMCAT_SI_VSLS	Yes	No	Yes	Seasonal
pTOMCAT_OO_VSLS	No	Yes	Yes	Seasonal
pTOMCAT_Fixed_DF	Yes	Yes	Yes	Fixed
UKCA__SI_OO_VSLS	Yes	Yes	Yes	Seasonal
UKCA_VSLS	No	No	Yes	Seasonal
UKCA_SI_VSLS	Yes	No	Yes	Seasonal
UKCA_OO_VSLS	No	Yes	Yes	Seasonal

Table 3. Correlation coefficients (R) at each site between various variables used in Fig. 6 and 7. Note that [*] indicates probability value < 0.1, [**] <0.01 and [***] < 0.001.

R	Obs O_3 vs model surface O_3	Obs O_3 vs model $BrO_{surface}$	Obs O_3 vs model BrO_{trop}	Obs O_3 vs GOME-2 BrO_{trop}	Model surface O_3 vs model $BrO_{surface}$	Model BrO_{trop} vs GOME-2 BrO_{trop}	Model BrO_{trop} vs model $BrO_{surface}$
Ticksi	0.68[***]	-0.49[***]	-0.53[***]	-0.62[***]	-0.78[***]	0.59[***]	0.96[***]
Barrow	0.49[***]	-0.04	-0.23[***]	-0.32[**]	-0.42[***]	0.37[***]	0.87[***]
Summit	0.63[***]	-0.19[***]	0.03	0.09	0.00	0.16[*]	0.42[***]
Villum	0.76[***]	-0.51[***]	-0.34[***]	-0.42[***]	-0.50[***]	0.33[**]	0.57[***]
Alert	0.24[***]	-0.05[*]	-0.22[***]	0.03	-0.36[***]	0.30[**]	0.59[***]
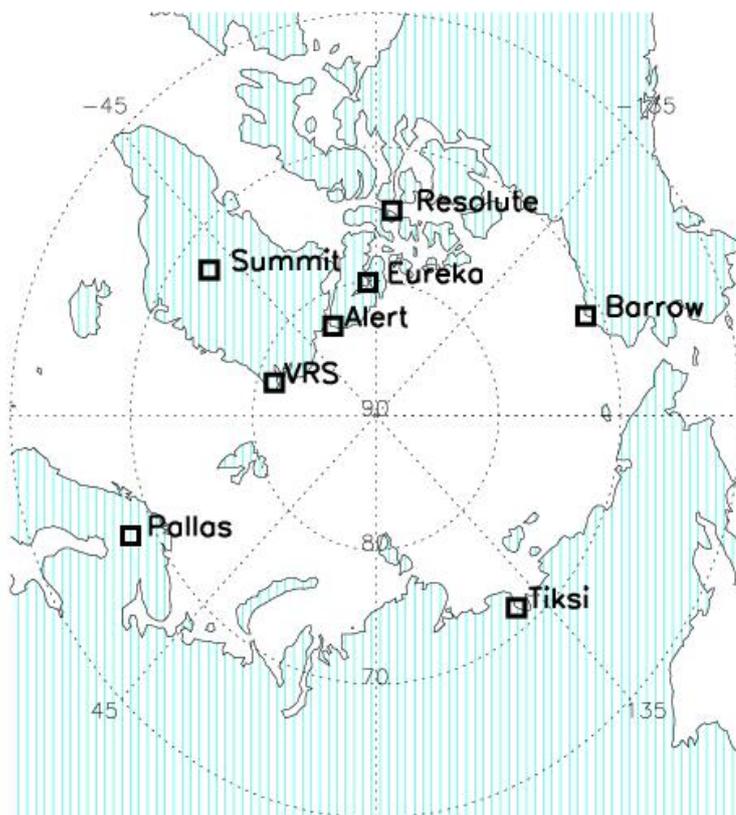
Figure1: Map of the Arctic showing the locations of the eight Arctic sites where either surface ozone and/or ozonesonde data are used in this study.
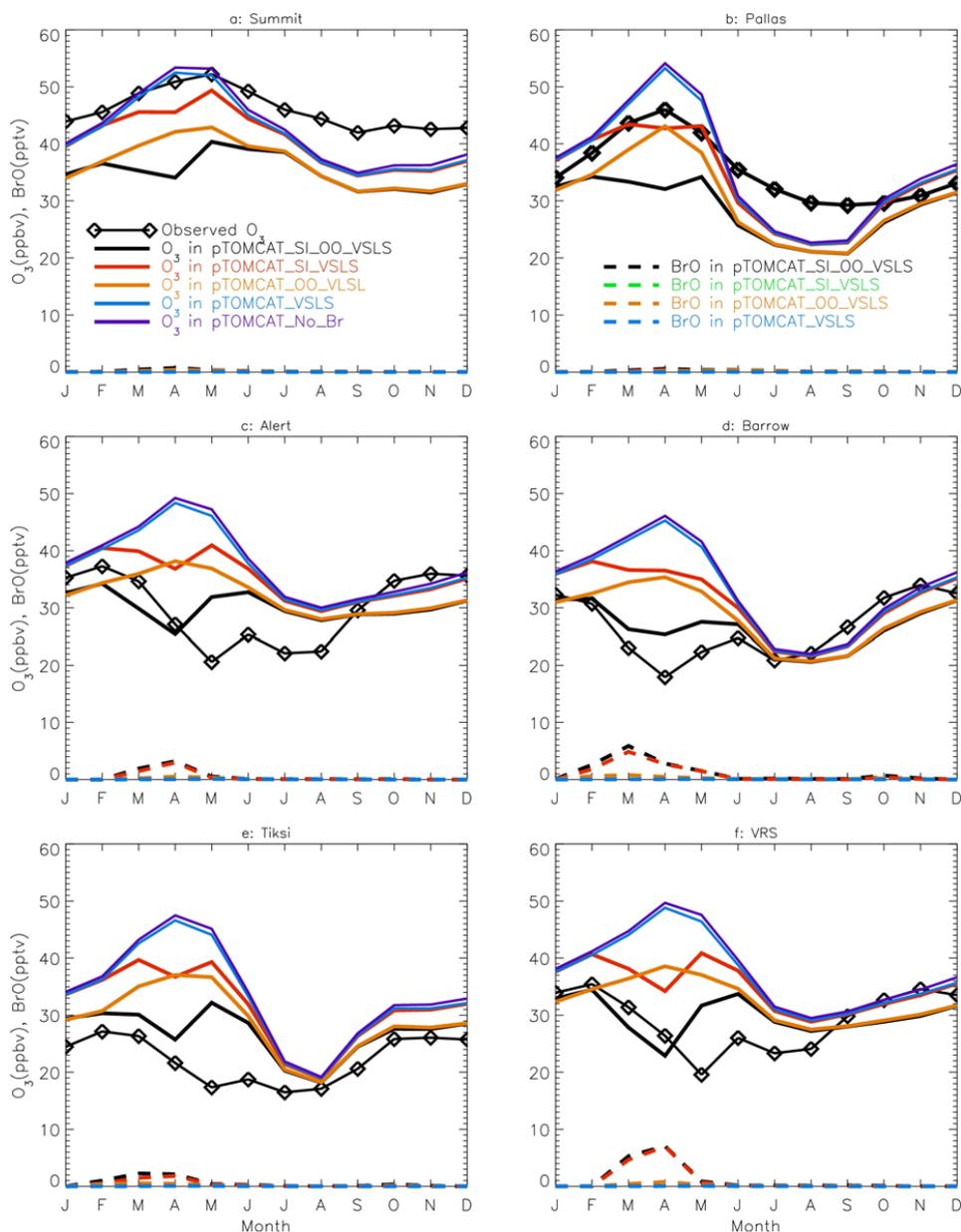
Figure 2: Climatology of monthly mean surface ozone (solid black line with diamond symbols) at six Arctic sites. The observed data are the average of 2000-2016 at Summit, 1995-2012 at Pallas, 1992-2012 at Alert, 1974-2016 at Barrow, 2011-2016 at Tiksi and 1980-2014 at VRS Research Station. Model surface ozone concentrations (VMRs) from various experiments are

5   shown in colourful solid lines with BrO in dashed lines based on an integration of 2006-2008.
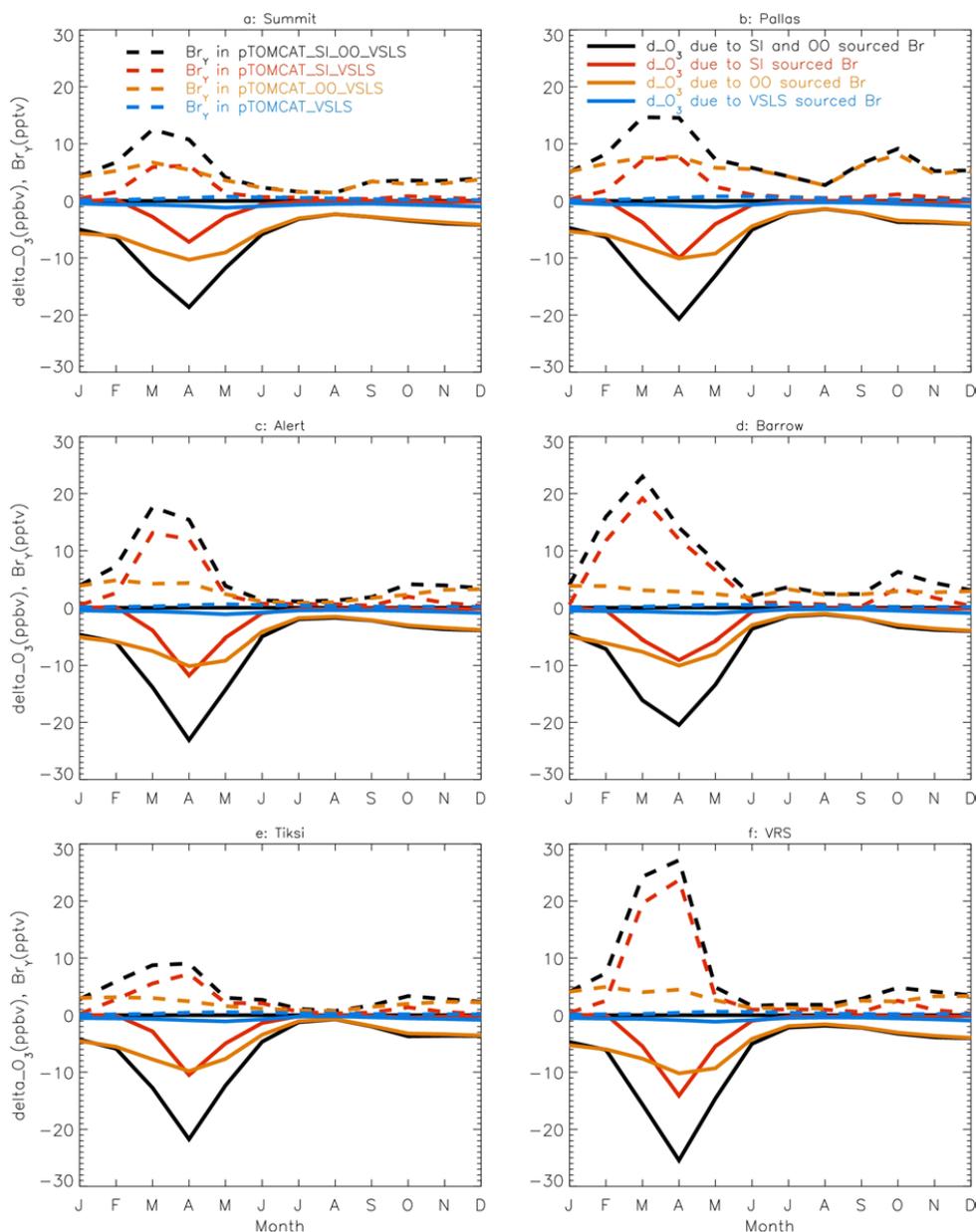
Figure 3: Ozone changes in response to alteration of various bromine sources. E.g., solid black line =pTOMCAT_SI_OO_VSLS - pTOMCAT_VSLS representing both SI and OO contributions, solid red line =pTOMCAT_SI_OO_VSLS - pTOMCAT_OO_VSLS representing SI contribution only, solid orange line =pTOMCAT_SI_OO_VSLS - pTOMCAT_SI_VSLS representing OO contribution only, and solid blue line =pTOMCAT_VSLS - pTOMCAT_No_Br representing VSLS contribution only. Dashed lines represent total inorganic bromine (Br_Y) in various model runs: the dashed black line is the pTOMCAT_SI_OO_VSLS run representing all bromine source contributions, the dashed red line is the pTOMCAT_SI_VSLS run representing SI and VSLS contributions, the dashed orange line is the pTOMCAT_OO_VLSL run representing OO and VSLS contributions, and the dashed blue line is the pTOMCAT_VSLS run representing VSLS contribution only.
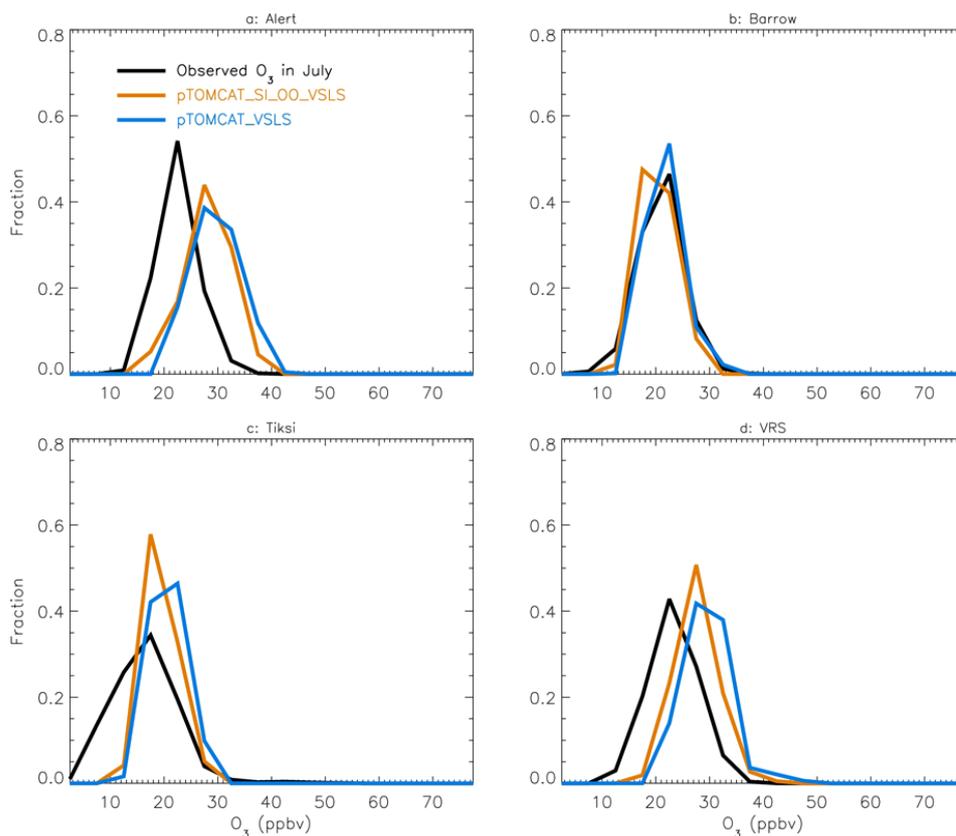
Figure 4: July surface ozone fractional distribution (with a bin interval of 5 ppbv). The observed fractional distribution is shown in black line, with pTOMCAT_SI_OO_VLS result shown in solid orange and pTOMCAT_VSLS shown in solid blue.
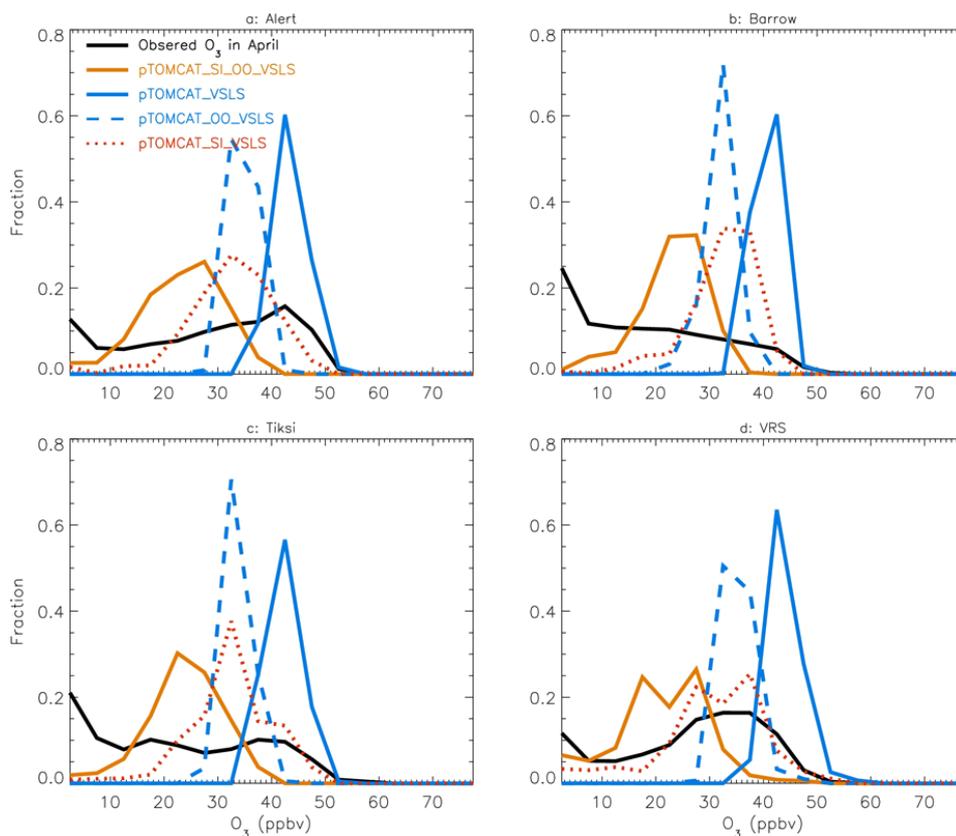
Figure 5: Same as Fig. 4 but for April. Also shown are the pTOMCAT_OO_VSLS results using dashed blue line and the pTOMCAT_SI_VSLS result in dashed orange.
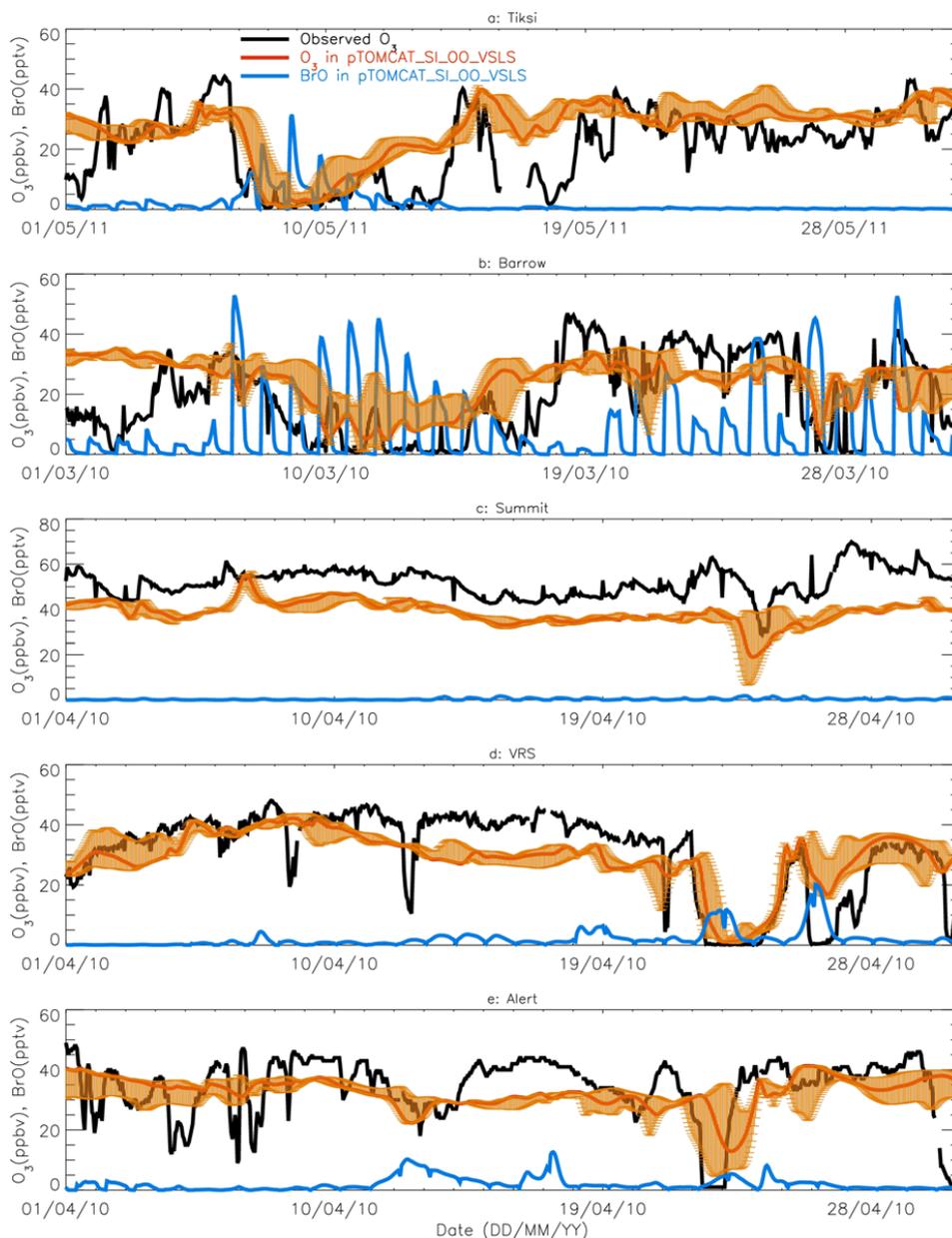
Figure 6: 1-month long time-series of surface ozone and BrO at (a) Tiksi (May 201), (b) Barrow (March 2010), (c) Summit (April 2010), (d) Villum (April 2010) and (e) Alert (April 2010). Observed ozone is shown in black, with pTOMCAT_SI_OO_VSLS ozone shown in bold red representing value of the nearest central gridbox to the observation site. The bold blue line is central gridbox BrO. Note that maximum and minimum ozone, which are shown in orange bars, are taken from the five adjacent gridboxes next to the central gridbox to highlight the possible range of the tracer concentrations.
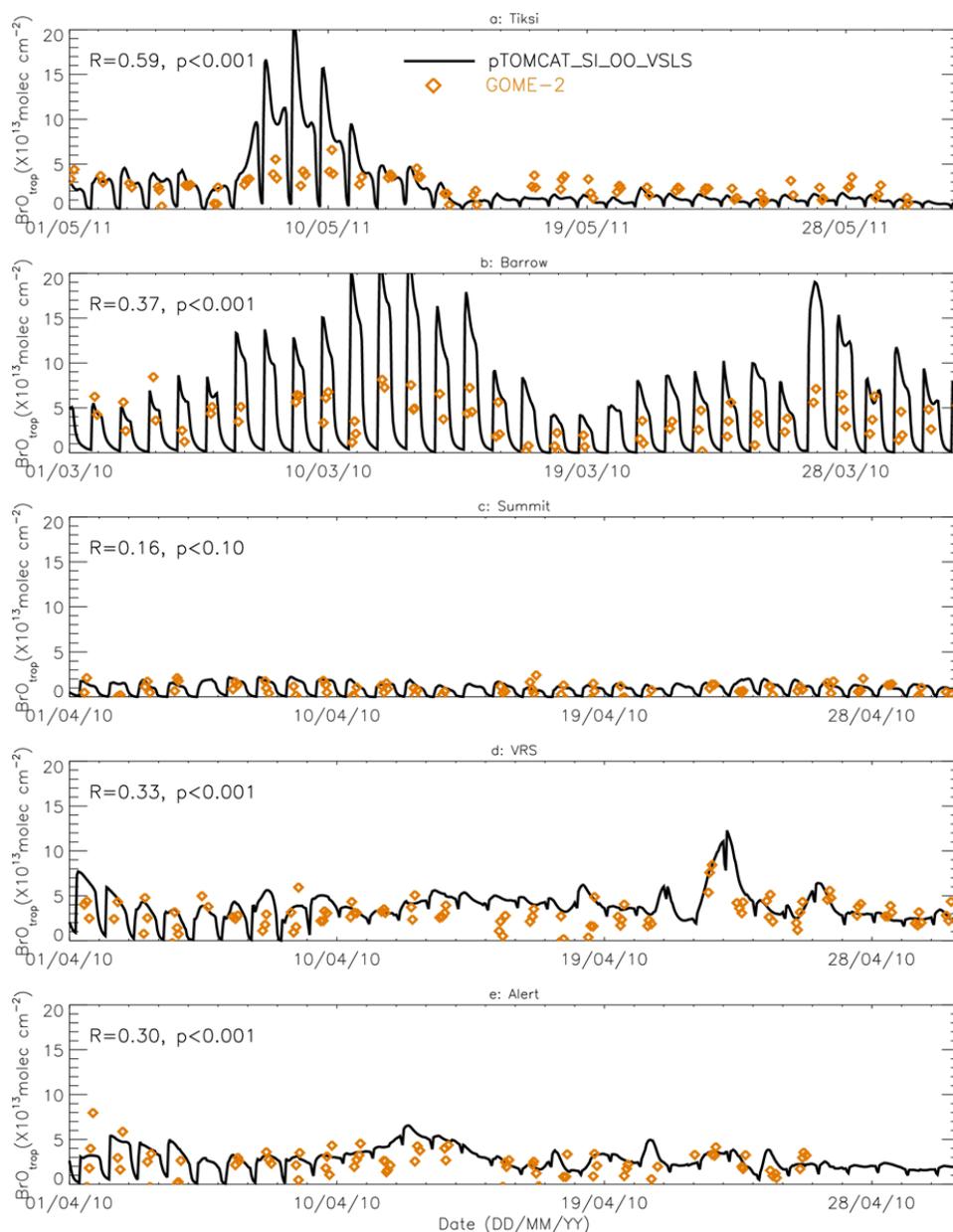
Figure 7: Time-series of tropospheric BrO column from GOME-2 (orange diamond symbols) and pTOMCAT_SI_OO_VSLS run BrO (black line). The correlation coefficient *R* and statistics significance level p at each site is given.
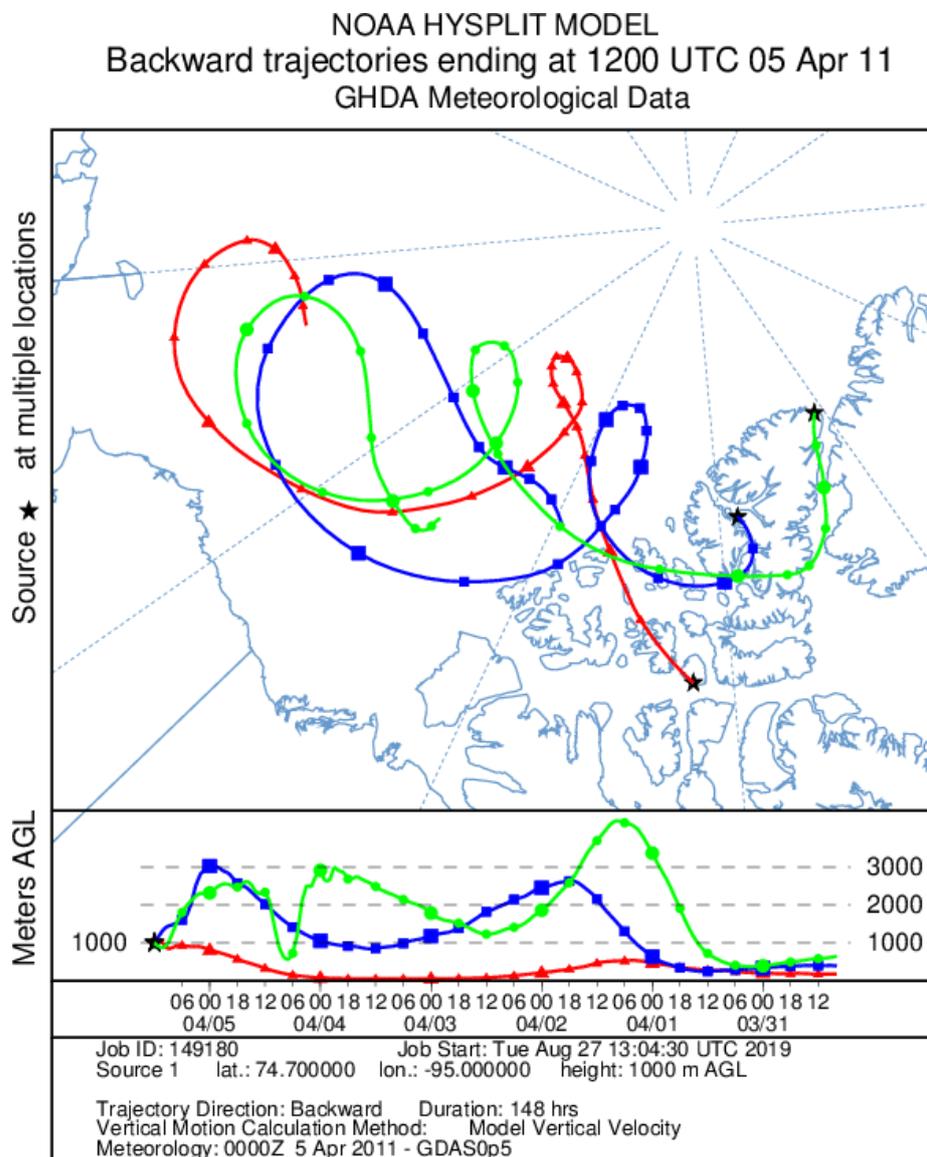
Figure 8: HYSPLIT 6-day back trajectories for Resolute, Eureka and Alert ending at 12:00 UTC on 5 April 2011.
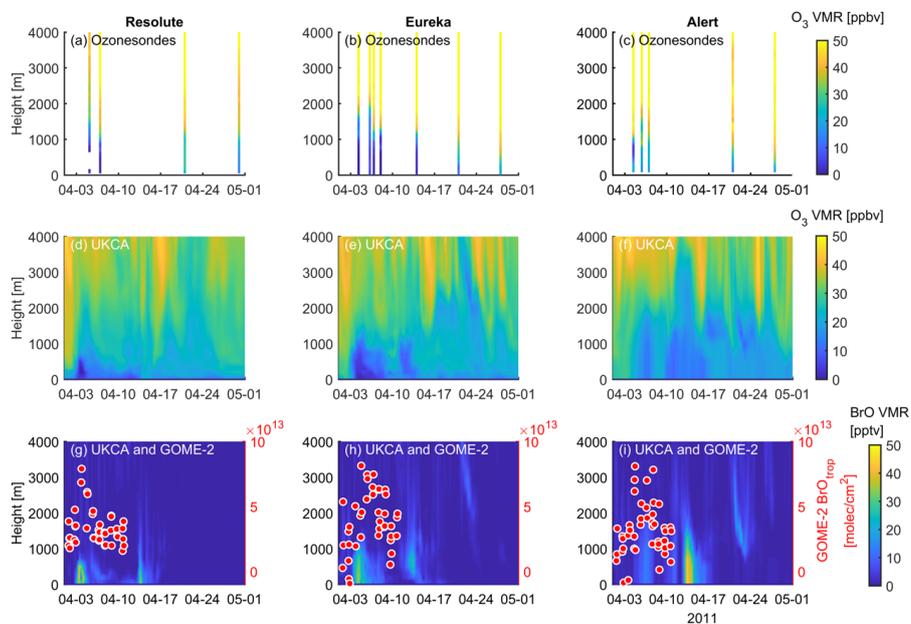
Figure 9: Profile of ozonesonde (0-4km) at Resolute (a), Eureka (b), and Alert (c) during April 2011. UKCA_Base ozone profiles (d-f) and BrO profiles (g-i) are also plotted. GOME-2 overpass data (tropospheric column BrO) of the period 1-10

5   April 2011 is also plotted in g-i, which is detailed in Fig. 10.
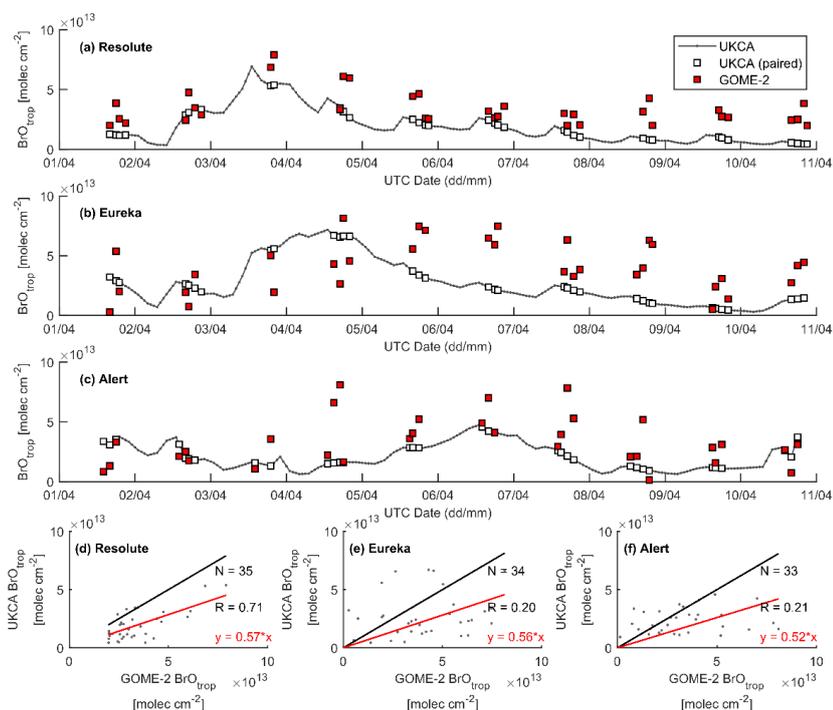
Figure 10: Time series of GOME-2 and UKCA_Base tropospheric BrO column at (a) Resolute, (b) Eureka, and (c) Alert for the period 1-10 April 2011. Correlation plots between the model and GOME-2 are shown in d-f, with black line representing 1:1 plot and red line representing regression fit.